IMMUNOLOGY

# Heightened apoptotic priming of vascular cells across tissues and life span predisposes them to cancer therapy–induced toxicities

**Johan K. E. Spetz[1,2,3], Mary H. C. Florido[1,2,3,4,5], Cameron S. Fraser[1,2,3], Xingping Qin[1,2,3], Jonathan Choiniere[1,2,3], Stacey J. Yu[1,2,3], Rumani Singh[1,2,3], Max Friesen[4,5]†, Lee L. Rubin[4,5], Joe-Elie Salem[6,7], Javid J. Moslehi[8], Kristopher A. Sarosiek[1,2,3,9]***



**Although major organ toxicities frequently arise in patients treated with cytotoxic or targeted cancer therapies, the mechanisms that drive them are poorly understood. Here, we report that vascular endothelial cells (ECs) are more highly primed for apoptosis than parenchymal cells across many adult tissues. Consequently, ECs readily undergo apoptosis in response to many commonly used anticancer agents including cytotoxic and targeted drugs and are more sensitive to ionizing radiation and BH3 mimetics than parenchymal cells in vivo. Further, using differentiated isogenic human induced pluripotent stem cell models of ECs and vascular smooth muscle cells (VSMCs), we find that these vascular cells exhibit distinct drug toxicity patterns, which are linked to divergent therapy–induced vascular toxicities in patients. Collectively, our results demonstrate that vascular cells are highly sensitive to apoptosis-inducing stress across life span and may represent a "weakest link" vulnerability in multiple tissues for development of toxicities.**

## INTRODUCTION

Cancers are typically treated with agents that induce cell death in malignant cells but can also damage normal cells and healthy tissues, frequently resulting in wide-ranging toxicities that can limit the use of potentially curative therapies (*1*, *2*). Even patients cured of their neoplasms face long-term morbidities that reduce quality of life and overall survival, including but not limited to impairments in neural, renal, hepatic, respiratory, musculoskeletal, and cardiovascular (CV) function (*3*). However, despite the clear importance of maximizing quality of life for cancer survivors, the mechanisms driving these toxicities are poorly understood (*4*, *5*).

Most anticancer therapies used clinically, including cytotoxic chemotherapies, ionizing radiation (IR), and targeted therapies, preferentially induce an apoptotic cell death in cancer cells by damaging ubiquitous cellular components or disrupting essential signaling pathways (*6*). The reliance of normal cells on these same components and pathways suggests that induction of apoptosis may also be responsible for healthy tissue toxicities caused by these agents (*6*, *7*). The intrinsic (mitochondrial) apoptosis pathway is triggered when a proapoptotic, pore-forming protein in the BCL-2 family (BAX or BAK) is activated by a BH3-only activator protein (e.g., BIM or BID) to trigger mitochondrial outer membrane permeabilization (MOMP) and consequent release of cytochrome c from mitochondria to activate caspases for cell dismantling (*8*). However, prosurvival proteins in this family (predominantly BCL-2, BCL-$X_L$, and MCL-1) can bind and block the activity of either the pore-forming proteins or BH3-only activators. The abundance of prosurvival and proapoptotic proteins varies between different cell types and differentiation stages and determines cell fate in response to apoptotic signals induced by damage or stress. This apoptotic sensitivity is referred to as "apoptotic priming" and can be measured via BH3 profiling, a functional assay that quantifies cytochrome c release in response to titrated doses of proapoptotic BH3 peptides in permeabilized cells (*9*). Because the commitment to intrinsic apoptosis is based on the interactions between more than 20 prosurvival and proapoptotic BCL-2 family proteins, a functional measurement of overall apoptotic sensitivity is required to accurately determine the cellular predisposition to apoptosis. Apoptotic priming is a critical determinant of cell fate in response to chemotherapy or radiation in both cancer cells (*7*, *10*–*13*) and healthy tissues (*14*).

Previous studies have revealed that cells comprising most of many somatic tissues including the brain, heart, liver, and kidneys are primed for apoptosis in early life but become apoptosis refractory by adulthood, while cells of hematopoietic origin remain similarly primed for apoptosis throughout life (*14*). This apoptotic resistance in adult somatic tissues suggests that the toxicities induced by cancer therapies are mediated either by nonapoptotic forms of cell death or by the induction of apoptosis in other critical supportive cell types (*15*). Vascular smooth muscle cells (VSMCs) and endothelial cells (ECs) are the major constituents of blood vessels and, when functional, control the flow of nutrients and waste products into and out of a tissue. Because of the critical role of the blood vasculature, its disruption can cause impairment of tissue function even if parenchymal cells are fully intact (*4*). Furthermore, CV toxicities are a major complication of cancer treatment and are the leading noncancer

[1]John B. Little Center for Radiation Sciences, Harvard T.H. Chan School of Public Health, Boston, MA, USA. [2]Laboratory of Systems Pharmacology, Harvard Program in Therapeutic Science, Department of Systems Biology, Harvard Medical School, Boston, MA, USA. [3]Molecular and Integrative Physiological Sciences Program, Harvard T.H. Chan School of Public Health, Boston, MA, USA. [4]Department of Stem Cell and Regenerative Biology, Harvard University, Cambridge, MA, USA. [5]Harvard Stem Cell Institute, Harvard University, Cambridge, MA, USA. [6]Clinical Investigation Center Paris-Est, CIC-1901, INSERM, UNICO-GRECO Cardio-Oncology Program, Department of Pharmacology, Pitié-Salpêtrière University Hospital, Sorbonne Université, Paris, France. [7]Cardio-Oncology Program, Department of Medicine, Vanderbilt-Ingram Cancer Center, Vanderbilt University School of Medicine, Nashville, TN, USA. [8]Section of Cardio-Oncology and Immunology, Division of Cardiology and the Cardiovascular Research Institute, University of California San Francisco, San Francisco, CA, USA. [9]Department of Medical Oncology, Dana-Farber Cancer Institute/Harvard Cancer Center, Boston, MA, USA.
*Corresponding author. Email: sarosiek@hsph.harvard.edu
†Present address: Whitehead Institute for Biomedical Research, Cambridge, MA, USA.

cause of death in cancer survivors (*3*), offsetting the therapeutic benefits to tumor control. The contribution of cancer treatment–induced dysfunction and death of cardiomyocytes in the development of cardiac toxicities has been well established (*5*, *15*–*18*). However, the study of therapy-induced vascular dysfunction has been challenging because of the heterogeneous clinical presentation of symptoms in terms of severity and timing, as well as the lack of rigorous in vitro models that accurately recapitulate patient experiences (*5*).

Here, we sought to elucidate how apoptosis is regulated in ECs and VSMCs to evaluate their vulnerability to apoptosis-inducing cancer therapeutics and potential roles in therapy-induced vascular toxicity. Notably, we find that these cell types maintain a high level of apoptotic priming throughout life span and, consequently, undergo apoptosis in response to commonly used chemotherapies, IR, novel BH3 mimetics, and targeted agents in a divergent manner. These differences in sensitivity are associated with specific drug-induced vascular toxicities in patients, while their heightened priming relative to parenchymal cells may drive toxicities more broadly.

## RESULTS

### Vascular ECs are primed for apoptosis throughout life, even in otherwise refractory tissues

To uncover potential cellular vulnerabilities to apoptosis-inducing anticancer therapies within healthy tissues, we used BH3 profiling to measure apoptotic priming at the single-cell level across major tissues from birth to adulthood. We collected tissue from key organs that experience cancer therapy–induced toxicities including liver, lung, heart, and kidney from mice in different stages of postnatal development [postnatal days 0 to 85 (P0 to P85); Fig. 1A and fig. S1A]. We dissociated the tissues and stained cells for CD31 (PECAM-1) to label ECs, CD45 to label peripheral blood mononuclear cells (PBMCs), and markers of parenchymal cell types in each tissue [EPCAM for epithelial cells in kidney and lung, cardiac troponin (cTnT) for cardiomyocytes in heart, and GLUT2 for hepatocytes in liver]. We then measured priming in each cell by detecting the release of mitochondrial cytochrome c (indicating initiation of apoptosis) in response to proapoptotic BH3 peptide treatments.

In agreement with our previous reports (*14*), we found that unlabeled cells that constitute most of the cells within each tissue (CD45 and CD31 negative) release cytochrome c in response to treatment with even low concentrations of proapoptotic BIM BH3 peptide [which can inhibit all of the prosurvival BCL-2 family proteins and directly activate BAX and/or, to a lesser degree, BAK (*10*)] in early life, indicating that they are primed for apoptosis (Fig. 1B). This priming was lost in most tissues as the mouse transitioned to adulthood. When analyzing labeled parenchymal cells, we found that these closely mimicked the priming levels of the unlabeled cells, indicating that the parenchymal cells make up the bulk of our previously reported apoptotic priming measurements (*14*). Among these, hepatocytes, cardiomyocytes, and kidney epithelial cells were far less primed in adult animals and nearly completely insensitive to even high concentrations of BIM and BID BH3 peptides (100 μM; Fig. 1B and fig. S1B, with the exception of 100 μM BID in liver). Similar resistance to proapoptotic BH3 peptides was evident in adult liver cells by directly assessing cytochrome c release from mitochondria by Western blotting (fig. S1C). In addition, in accordance with previous findings (*19*), $CD45^+$ PBMCs were consistently primed for apoptosis across life span. Unexpectedly, we also detected that the mitochondria of $CD45^-/CD31^+$ ECs maintained a high level of priming across the studied ages (Fig. 1B), with only a mild decrease being evident when comparing ECs in adult versus young mice (fig. S1, E and F). The priming in ECs is more similar to PBMCs than parenchymal cells. These results indicate that while most cells in adult liver, kidney, heart, and (to some extent) lung lose their apoptotic sensitivity, ECs retain a similar level of apoptotic priming throughout life, independent of the priming of cells in surrounding tissues. Further, using a normalized area under the curve (AUC) calculation for the BH3 peptide treatment responses, we found that apart from PBMCs, ECs were the most primed cells of those we investigated (Fig. 1C and fig. S1D).

### ECs undergo apoptosis in response to cytotoxic treatment in vivo

We reasoned that the relatively high apoptotic priming of ECs may predispose them to being vulnerable to traditional cancer therapeutics such as IR, as has been established previously for cancer cells as well as cells from developing tissues (*7*, *14*). In patients, radiation therapy can cause a wide range of healthy tissue toxicities including vascular diseases (*4*). We therefore sought to test whether ECs underwent apoptosis in response to IR in vivo at rates consistent with their level of apoptotic priming, especially relative to the lower priming of parenchymal cells. We treated P70 mice with 8-Gy whole-body γ-irradiation and measured apoptosis induction using both flow cytometry on isolated cells and immunofluorescence microscopy on tissue sections (Fig. 1D). Using annexin V (AxV) staining, we found that $CD45^+$ PBMCs and $CD31^+$ ECs underwent apoptosis after irradiation in a time-dependent manner, as predicted by BH3 profiling (Fig. 1, E to H). We also confirmed these results by measuring caspase-3/7 activity and plasma membrane integrity (fig. S2). We next sought to measure the extent of apoptosis induction by IR in intact tissues by performing tissue immunofluorescence microscopy using anti-CD31 and anti–cleaved caspase-3 (Cl-Casp3) on liver, kidney, heart, and lung tissue collected 12 hours after 24-Gy irradiation (Fig. 2, A to D). Quantification of the number of $CD31^-/Cl\text{-}Casp3^+$ and $CD31^+/Cl\text{-}Casp3^+$ cells revealed that 24-Gy γ-irradiation resulted in a significantly higher number of $Cl\text{-}Casp3^+$ cells in $CD31^+$ ECs in all four tissues, while for $CD31^-$ cells there was only a significant increase of $Cl\text{-}Casp3^+$ cells in the lung (Fig. 2, E to H). These results demonstrate that ECs are more sensitive to γ-irradiation than parenchymal cells in many adult tissues. The death of vascular ECs in response to cancer therapeutics such as IR may constitute the initiating factor in the development of long-term tissue dysfunction.

### Vascular ECs express high levels of proapoptotic BCL-2 family member genes

To characterize which BCL-2 family proteins maintain heightened EC apoptotic priming in adult mice, we analyzed single-cell gene expression data from the Tabula Muris database (*20*) and compared the expression of genes involved in intrinsic apoptosis in ECs and parenchymal cells from adult mouse kidney, liver, lung, and heart (Fig. 2I). We found that although there were some differences in apoptosis gene expression between ECs from different tissues, the key pore-forming proapoptotic proteins BAX and BAK (encoded by *Bax* and *Bak1*, respectively) were expressed at higher levels than in parenchymal cells. Notably, heart VSMCs had a more similar gene expression pattern to ECs than to cardiomyocytes, indicating that VSMCs are expected to regulate apoptosis similarly to ECs in vivo. These

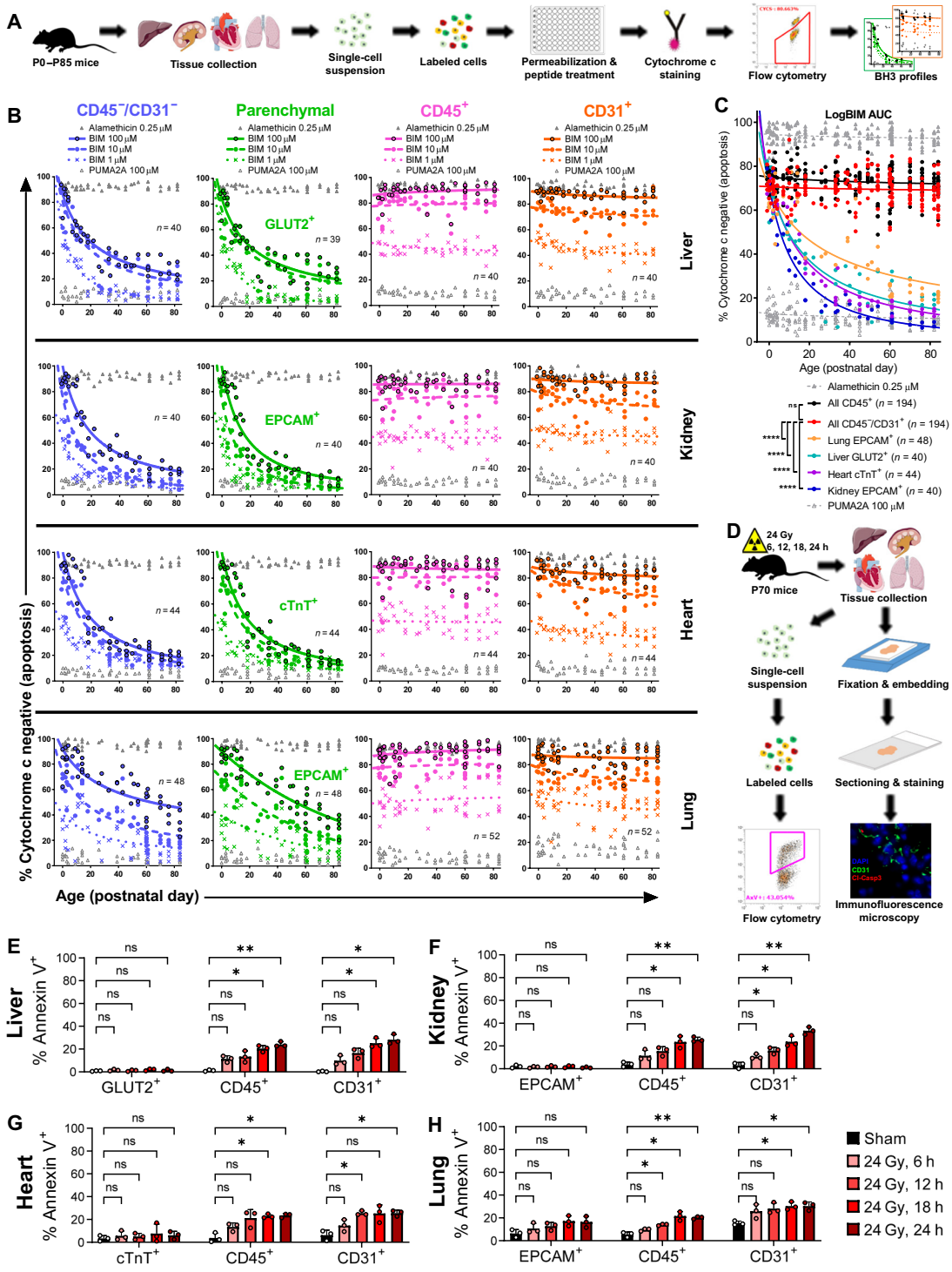


**Fig. 1. Vascular ECs are primed for apoptosis throughout life, even in otherwise refractory tissues.** (**A**) Schematic of tissue BH3 profiling. Cells were isolated from heart, liver, lung, and kidney tissue from postnatal mice of different ages. Cells were stained with markers for ECs (CD31), PBMCs (CD45), and parenchymal cells (cTnT, GLUT2, or EPCAM) and BH3-profiled. Cytochrome c–negative cells were identified in nucleated cells ($DAPI^+$) using a cytochrome c antibody. (**B**) Summary BH3 profiling data for parenchymal, $CD45^+$, and $CD31^+$ cells for three different concentrations of BIM BH3 peptide across tissues during postnatal development. Each data point indicates data from one tissue specimen. (**C**) Normalized BIM AUC profiles comparing priming of $CD45^+$ and $CD31^+$ cells from all tissues studied with parenchymal cells from each tissue. Each data point indicates data from one tissue specimen. Alamethicin is positive control; PUMA2A is negative control. Significance: ns, not significant, $^{****}P < 0.0001$. (**D**) Schematic of in vivo cytotoxic treatments. P70 mice were irradiated with 24-Gy whole-body γ-radiation, and liver, kidney, heart, and lung tissues were collected. Cells were isolated from tissue samples after 6, 12, 18, and 24 hours and stained with CD31, CD45, and parenchymal markers, and AxV positivity was measured by flow cytometry. Separate tissue samples were processed for immunofluorescence microscopy (described in Fig. 2). (**E** to **H**) Summary AxV positivity data from parenchymal, $CD45^+$, and $CD45^-/CD31^+$ cells from mice of different ages; $n = 3$ animals per treatment condition. Significance: ns, not significant, $^{**}P < 0.01$.

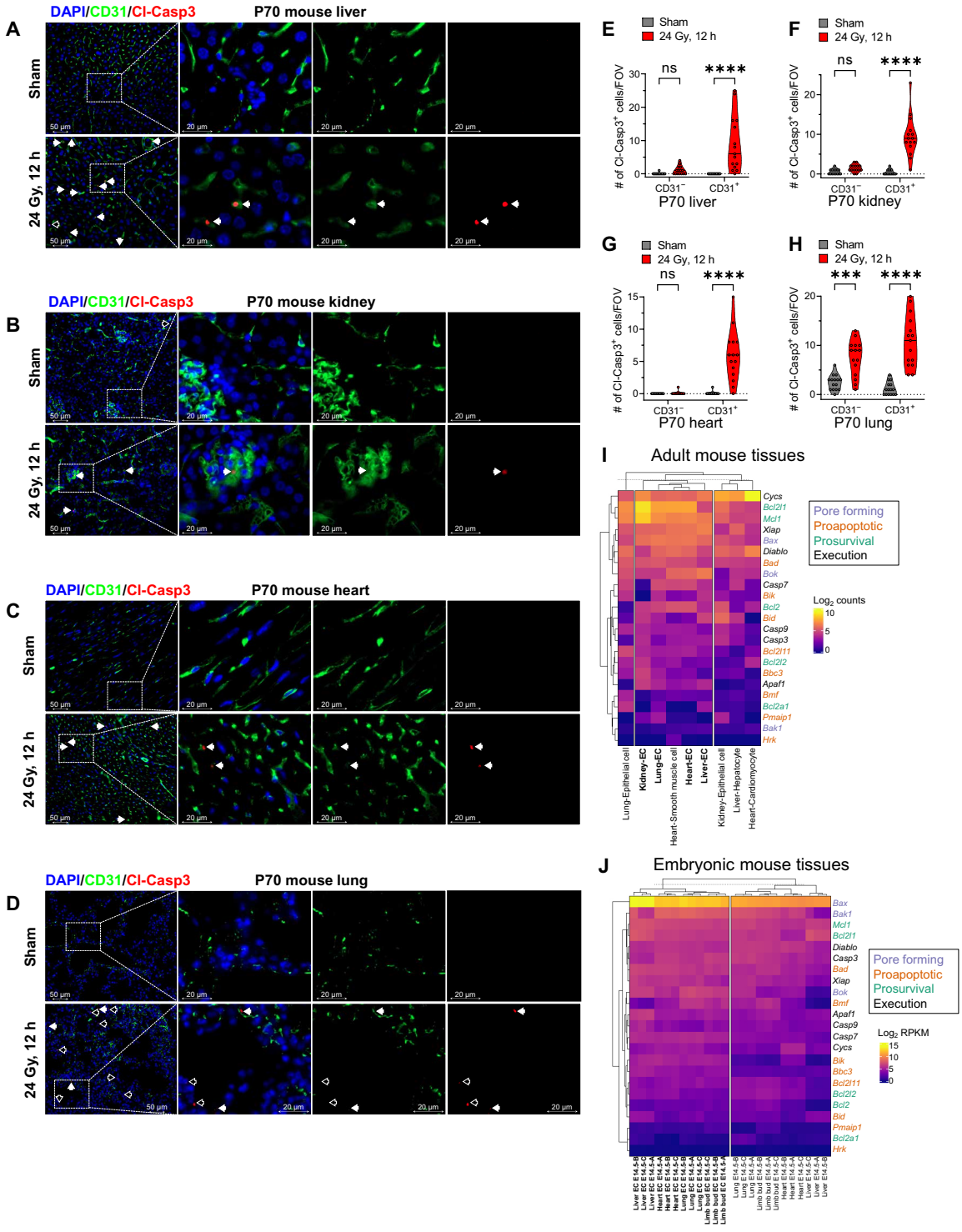


**Fig. 2. Vascular ECs undergo apoptosis in response to in vivo cytotoxic treatment and express high levels of proapoptotic BCL-2 family member genes.** (**A** to **D**) Representative images of immunofluorescence staining for CD31 and Cl-Casp3 in (A) liver, (B) kidney, (C) heart, and (D) lung from P70 mice 12 hours after either sham treatment or 24-Gy whole-body γ-irradiation. Filled arrowheads indicate examples of cells that are positive for both CD31 and Cl-Casp3; empty arrowheads indicate cells that are positive for only Cl-Casp3. $n = 3$ animals per treatment condition. (**E** to **H**) Quantification of number of Cl-Casp3$^+$ cells in CD31$^+$ or CD31$^-$ cells per 20× field of view from immunofluorescence images of sham or 24 Gy–irradiated (E) liver, (F) kidney, (G) heart, and (H) lung. $n = 15$ (3 animals per treatment condition, 5 images per animal). (**I** and **J**) Single-cell RNA-seq data for genes involved in mitochondrial apoptosis in ECs, VSMCs, and parenchymal cells of adult mouse heart, liver, lung, and kidney. Expression data mined from (I) the Tabula Muris database (*20*) and (J) Hupe *et al.* (*22*).

expression patterns were confirmed in an additional independent gene expression dataset (fig. S3A) (*21*). Correlational analysis comparing logBIM AUC measurements (from Fig. 1C) with expression levels of apoptosis genes (from Fig. 2I) demonstrated that higher cellular priming levels were most strongly correlated with higher expression of *Apaf1* ($R^2$ = 0.906; $P$ < 0.0001), *Bax* ($R^2$ = 0.823; $P$ < 0.0001), *Xiap* ($R^2$ = 0.641; $P$ < 0.0001), and *Mcl1* ($R^2$ = 0.525; $P$ < 0.0001) (fig. S3B). This is in agreement with our previous work showing that genes in the apoptosis pathway are frequently co-regulated: Cells with a primed apoptosis pathway such as those found in the hematopoietic system and parenchymal cells in young tissues typically express higher levels of proapoptotic and prosurvival proteins as well as higher levels of proteins involved in post-MOMP apoptosis execution such as APAF-1 and caspases (*14*).

Furthermore, by examining another published gene expression dataset using embryonic (E14.5) mouse tissues (*22*), we again found that *Bax* and *Bak1*, among other proapoptotic genes, were expressed in peripheral ECs of different origin and again at higher levels than in the remaining cells of those tissues (Fig. 2J). By comparing gene expression patterns of apoptosis-related genes across different tissues in both adult and embryonic mice, we see that while cells from the same tissue cluster together, all ECs cluster separately from the other cell types (except heart VSMCs), regardless of tissue of origin. This indicates that the intrinsic apoptosis pathway is similarly regulated in ECs and VSMCs across peripheral tissues and distinctly from the parenchymal cells of the tissues they support.

### The two major cell types of the vasculature, ECs and VSMCs, are primed for apoptosis in vitro

To further understand apoptotic regulation in the cells of the human blood vessel wall, we differentiated human induced pluripotent stem cells (hiPSCs) into vascular ECs and VSMCs using well-established protocols (*23*) and BH3-profiled them. We confirmed cellular identity of the differentiated cells via immunofluorescence staining for EC marker CD31 and VSMC marker α-smooth muscle actin (αSMA) (Fig. 3A). We also cultured primary human coronary artery endothelial cells (HCAECs) as a primary human cell control, human primary foreskin fibroblasts (FFs) for comparison with a nonvascular cell type, and HeLa cells for comparison with a commonly used cancer cell line. BH3 profiling revealed that while hiPSC-ECs were less primed for apoptosis than the parental hiPSCs, they were more primed than HCAECs and hiPSC-VSMCs (Fig. 3B). Nevertheless, the BH3 profiling results suggest that all these cells would be highly responsive to apoptosis-inducing stress and damage. FFs were largely insensitive to all BH3 peptide treatments, except the highest concentration of BIM BH3, indicating that they are unprimed. Last, vascular cells exhibited similar levels of priming to the HeLa cervical cancer cell line, which is known to undergo apoptosis in response to many cancer therapeutics (*10*).

We next sought to compare the regulation of apoptosis-related genes between hiPSC-derived cells and their tissue-isolated counterparts using RNA sequencing (RNA-seq) (Fig. 3C). We found that, in line with the mouse tissue data (Fig. 2, I and J, and fig. S3), hiPSC-ECs and hiPSC-VSMCs express relatively high levels of *BAX* and *BAK1*, especially compared with cells differentiated into a nonvascular lineage such as hiPSC-WAT (white adipose tissue) cells. Further, the lower levels of *BAX* and *BAK1* expression in hiPSC-WAT cells were consistent with their lower apoptotic priming compared with hiPSC-ECs (fig. S4A). In addition, in line with our BH3 profiling results, which showed the undifferentiated hiPSCs as being the most primed of the cell types, we saw that hiPSCs expressed the highest levels of both *BAX* and *BAK1*, as well as other proapoptotic BCL2 family members including *BBC3* (encoding PUMA), *HRK*, and *PMAIP1* (encoding Noxa). These differences were confirmed at the protein level: We found that hiPSCs and hiPSC-ECs express high levels of BAX and BAK, which were both found to be lower in hiPSC-WAT cells (Fig. 3D). Expression levels of signature genes for ECs and VSMCs across the hiPSC-derived cells confirmed the differentiation into each respective lineage (fig. S4B), as did the detection of vascular endothelial cadherin only in hiPSC-ECs at the protein level (Fig. 3D).

### ECs and VSMCs in vitro undergo apoptosis in response to standard chemotherapeutics and IR

Because we have previously found that apoptotic priming is a determinant of cancer cell sensitivity to cytotoxic stress (*7*, *10*–*13*), we hypothesized that ECs and VSMCs would be broadly sensitive to anticancer agents. To evaluate this, we treated HCAECs, hiPSC-derived vascular ECs and VSMCs, FFs, and HeLa cells with a panel of anticancer agents including IR and standard classes of cytotoxic chemotherapies. After a 48-hour treatment, we stained cells with AxV and propidium iodide (PI) to quantify live ($AxV^-/PI^-$), early apoptotic ($AxV^+/PI^-$), late apoptotic ($AxV^+/PI^+$), and degraded ($AxV^-/PI^+$) cells (Fig. 3I). For dose reference in comparison with clinical use, we searched the literature for maximum plasma concentration ($C_{max}$) in patients (table S1) and indicated in the figure which in vitro drug concentration is at a comparable level (blue arrowheads).

In agreement with BH3 profiling results, hiPSCs were highly sensitive to most drugs used. The two EC cultures and VSMCs underwent apoptosis in response to many compounds tested. In general, hiPSCs, hiPSC-ECs, and hiPSC-VSMCs were considerably more sensitive than the FFs to most drugs, and sensitivity profiles were predicted by BH3 profiling (i.e., hiPSCs being the most sensitive, followed by hiPSC-ECs, HeLa cells, HCAECs, VSMCs, and, finally, FFs, which were the least sensitive cell type), especially for the less selective agents [e.g., IR, cisplatin, carboplatin, ara-C (cytarabine), and staurosporine]. Although hiPSC-ECs and HCAECs are both human ECs, HCAECs were significantly less sensitive to more than half of agents tested (32 of 51 drugs, 63%) (fig. S4C), which is consistent with their lower level of priming and again demonstrates that while ECs regulate apoptosis similarly across tissues, they should not be considered identical. Few drugs induced apoptosis in FFs and, then, only at high doses. In addition, consistent with their lower apoptotic sensitivity as measured by BH3 profiling, we found that hiPSC-WAT cells were resistant to a representative panel of these anticancer agents (fig. S4D). Although hiPSC-ECs were more sensitive in general than hiPSC-VSMCs, several drugs exhibited divergent efficacy between the two cell types that could not be explained by differences in apoptotic priming. Doxorubicin, mitoxantrone, and topotecan (which all inhibit topoisomerases), for example, showed higher apoptosis induction in hiPSC-VSMCs than in either of the EC cell types, indicating a mechanism of apoptosis induction from these drugs upstream of BCL-2 family proteins that is more active in VSMCs than in ECs. Furthermore, while alkylating agents and DNA synthesis inhibitors exhibited lower or comparable killing of both ECs and VSMCs compared with HeLa cells, ECs were significantly more sensitive than VSMCs. Note that across nearly all drug treatments tested, we detected large populations of $AxV^+/PI^-$ cells,

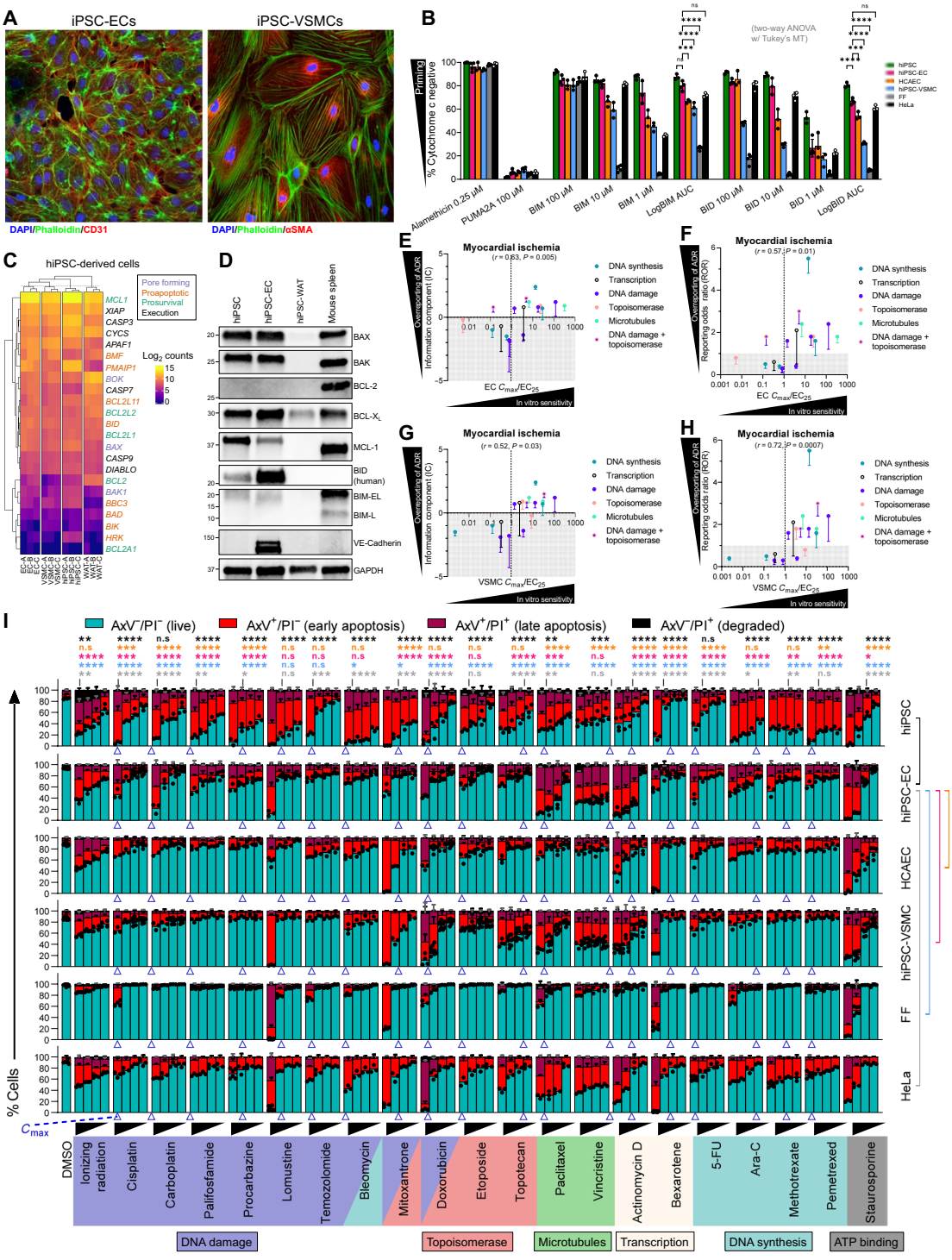


**Fig. 3. hiPSC-derived ECs and VSMCs are primed for apoptosis and sensitive to standard chemotherapeutics and IR.** (**A**) Immunofluorescence staining for EC marker CD31 and VSMC marker αSMA in cells differentiated from hiPSCs, counterstained for F-actin (phalloidin) and nuclei (DAPI). (**B**) BH3 profiling of hiPSC-derived, primary human, and HeLa cells; $n = 3$ to 4 biological replicates. (**C**) RNA-seq data for genes involved in mitochondrial apoptosis in hiPSCs, hiPSC-ECs, hiPSC-VSMCs, and hiPSC-derived WATs; $n = 3$ biological replicates. (**D**) Western blot showing expression of BCL-2 family proteins in hiPSCs, hiPSC-ECs, and hiPSC-WAT. VE-cadherin expression demonstrates endothelial lineage of hiPSC-ECs. Adult mouse spleen included for reference. (**E** to **H**) VigiBase overrepresentation of Myocardial ischemia shown as IC (E and G) or ROR (F and H) plotted against $C_{max}/EC_{25}$ of chemotherapeutics for hiPSC-ECs (E and F) and hiPSC-VSMCs (G and H). Error bars show lower end of 95% credibility and confidence intervals ($IC_{025}$ and $ROR_{025}$), respectively. Statistical significance was set at $IC_{025} > 0$ and $ROR_{025} > 1$, respectively. Correlation between IC or ROR and $C_{max}/EC_{25}$ was determined using Spearman's rank-order analysis. (**I**) AxV/PI staining of hiPSC-derived, primary human, and HeLa cells in response to IR and different classes of chemotherapeutics at four doses each, 48 hours after treatment start; $n = 3$ to 9 biological replicates. $C_{max}$ arrows indicate which concentration is comparable to maximum patient plasma concentration. Significance: ns, not significant, $^{*}P < 0.05$, $^{**}P < 0.01$, $^{***}P < 0.001$, and $^{****}P < 0.0001$.

indicating that phosphatidylserine exposure (an early indicator of apoptosis induction) occurred before membrane disruption—this confirms that these cell types are dying via canonical, caspase-mediated apoptosis in response to these agents. Similar patterns of sensitivity were observed at 24 and 72 hours (fig. S4, E and F).

To determine whether in vitro apoptosis induction of ECs or VSMCs was associated with vascular toxicities in patients, we performed a disproportionality analysis using the international pharmacovigilance database, VigiBase (*24*, *25*). Using individual case safety reports, we compared clinical overreporting of the adverse drug reaction (ADR) Myocardial ischemia [classified with the Medical Dictionary for Regulatory Activities (MedDRA)] versus the full database of events worldwide. We used the information component (IC; a Bayesian estimator, which compares disproportionality of observed versus expected ADR-drug count) and reporting odds ratio (ROR; a frequentist disproportionality estimator) (*25*, *26*) to determine which ADRs were significantly overreported. To relate these metrics to our in vitro results, we divided the $C_{max}$ of each of drug by the $EC_{25}$ (25% maximal effective concentration or concentration that induces apoptosis in 25% of cells) for hiPSC-ECs and hiPSC-VSMCs. A $C_{max}/EC_{25}$ ratio above 1.0 indicates that the dose used clinically induces apoptosis in >25% of vascular cells (EC or VSMC) in vitro, suggesting that those vascular cells would also undergo apoptosis in patients that are treated with that particular agent. This analysis demonstrated that drugs that induce apoptosis in ECs and/or VSMCs in vitro ($C_{max}/EC_{25} > 1$) are associated with the overreporting of Myocardial ischemia events in patients (Fig. 3, E to H, and table S1). Thus, in vitro EC or VSMC sensitivity to certain agents may portend toxicities in the clinic and provide insight into their cellular drivers.

## ECs and VSMCs in vitro are dependent on prosurvival BCL-2 family members BCL-$X_L$ and MCL-1 for survival

Having established that vascular cells are sensitive to proapoptotic stimuli in the form of BH3-only activator peptides or apoptosis-inducing drugs, we next sought to assess whether ECs and VSMCs are dependent on prosurvival proteins to buffer endogenous proapoptotic proteins. To do this, we measured cytochrome c release in response to sensitizer BH3 peptides, which can only induce MOMP by inhibiting the activity of specific prosurvival BCL-2 family proteins and freeing any actively bound proapoptotic BH3-only activator proteins (e.g., BIM or BID). iPSCs, hiPSC-derived ECs, VSMCs, and primary HCAECs were sensitive to treatment with the PUMA peptide (Fig. 4A), which inhibits all prosurvival proteins, indicating that they are broadly dependent on these proteins for survival [note that, unlike PUMA protein, the PUMA BH3 peptide is unable to directly activate BAX and BAK (*9*)]. We then measured responses to the BAD BH3 (inhibits BCL-2, BCL-$X_L$, and BCL-w), HRK BH3 (inhibits BCL-$X_L$), and MS1 (inhibits MCL-1) peptides. We saw similar moderate levels of cytochrome c loss in responses to all three peptides in hiPSC-derived ECs, VSMCs, and primary HCAECs, suggesting that they are somewhat dependent on each of the prosurvival proteins inhibited by these peptides. These results point to a dependence on BCL-2, BCL-$X_L$, and MCL-1 to sequester proapoptotic BH3-only activator proteins for survival in ECs and VSMCs and a potential vulnerability to apoptotic cell death should these proteins be inhibited or degraded, especially concurrently.

A novel class of anticancer drugs called BH3 mimetics has been recently developed to directly target prosurvival BCL-2 family proteins to induce apoptosis in cancer cells that are dependent on them.

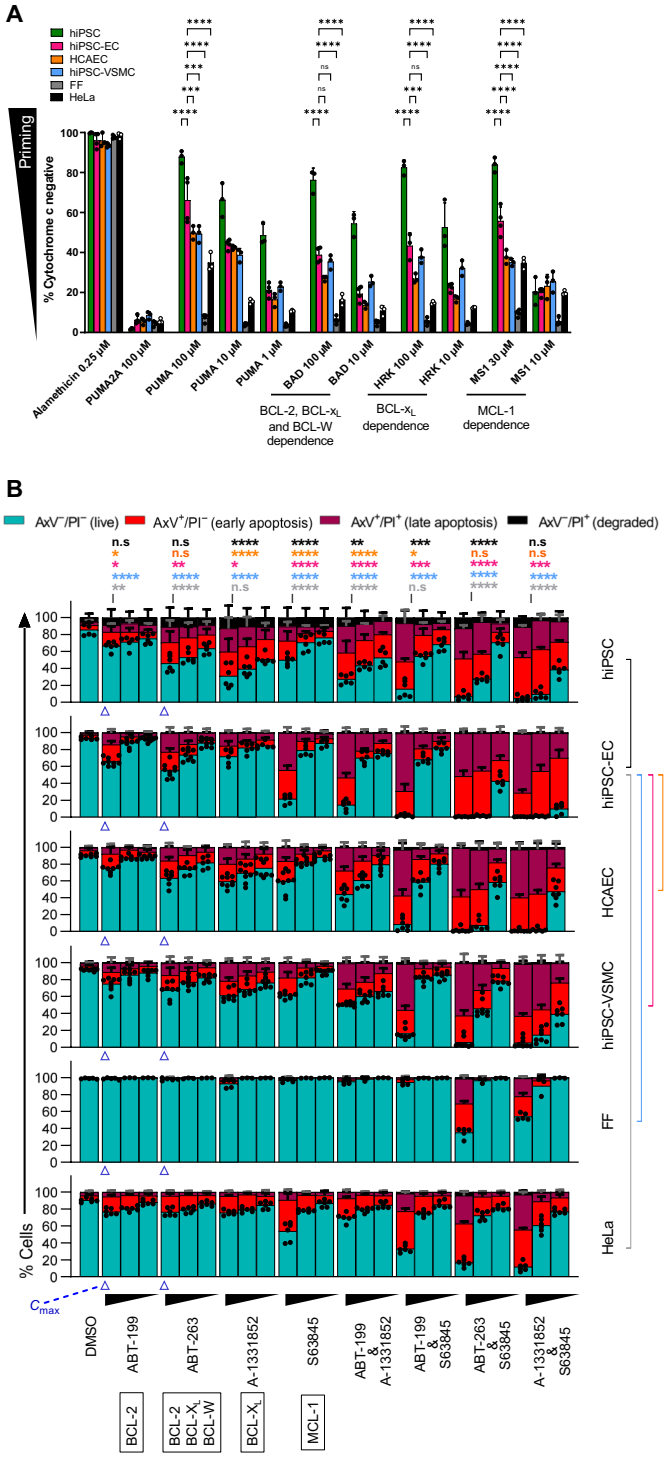


**Fig. 4. Vascular cell types are vulnerable to inhibition of prosurvival BCL-2 family proteins.** (**A**) BH3 profiling of hiPSCs, hiPSC-ECs, hiPSC-VSMCs, primary HCAECs, primary human FFs, and HeLa cells for sensitizer BH3 peptides BAD, HRK, MS1, and PUMA; $n = 3$ to 4 biological replicates. (**B**) AxV/PI staining of hiPSCs, hiPSC-ECs, hiPSC-VSMCs, HCAECs, FFs, and HeLa cells in response to BH3 mimetics alone or in combination, 24 hours after treatment start. All combinations were performed with the same concentration of each drug, and treatment was given simultaneously; $n = 3$ to 8 biological replicates. $C_{max}$ arrows indicate what concentration is comparable to maximum patient plasma concentration. Significance: ns, not significant, $^*P < 0.05$, $^{**}P < 0.01$, $^{***}P < 0.001$, and $^{****}P < 0.0001$.

Several different BH3 mimetics have been developed with selectivity for specific prosurvival proteins, e.g., ABT-199 (venetoclax, inhibiting BCL-2), ABT-263 (navitoclax, inhibiting BCL-2, BCL-$X_L$, and BCL-w), A-1331852 (inhibiting BCL-$X_L$), and S63845 (inhibiting MCL-1). The recent U.S. Food and Drug Administration (FDA) approval and successful use of ABT-199 in several hematologic malignancies have increased the interest in further development of BH3 mimetics. However, our limited clinical experience with these agents, especially when used in combinations, make it critical to identify potential toxicities that may arise from their use.

To test whether BH3 mimetics have cytotoxic effects on ECs and VSMCs, we measured induction of apoptosis in hiPSC-ECs, hiPSC-VSMCs, and HCAECs treated with BH3 mimetics as single agents and in combination for 24 hours (Fig. 4B). We found that, in line with the prediction from BH3 profiling, inhibition of BCL-2, BCL-$X_L$ , or MCL-1 alone induced mild but detectable levels of apoptosis in hiPSCs, hiPSC-ECs, hiPSC-VSMCs, and HCAECs. In line with previous reports (*27*), HeLa cells were only sensitive to S63845 among single-agent treatments. Notably, combining the BH3 mimetics greatly enhanced apoptosis induction in vascular cells, especially when combining BCL-$X_L$ and MCL-1 inhibition. A similar pattern of sensitivity was observed at 48 and 72 hours (fig. S5). These results indicate that targeting MCL-1 alone or in combination with BCL-$X_L$ is likely to result in substantial vascular toxicities, as would be targeting prosurvival proteins while also treating with other apoptosis-inducing, vascular toxic agents identified here.

## EC and VSMC responses to BH3 mimetics reveal vulnerabilities in vivo, especially to combinations of MCL-1 and BCL-$X_L$ inhibition

To compare our in vitro BH3 profiling results with sensitizer BH3 peptides with in vivo vascular ECs, we performed BH3 profiling on isolated cells from P0 to P85 mouse liver, kidney, heart, and lung (Fig. 5, A to D). Similar to in vitro results, ECs from all four tissues were sensitive to PUMA BH3 peptide treatment and somewhat sensitive to BAD BH3, HRK BH3, and MS1 peptides, indicating a potential vulnerability of ECs to BH3 mimetics.

To investigate whether BH3 mimetics induce apoptosis in ECs in vivo, we treated P70 mice with A-1331852, S63845, and a combination of both drugs and monitored the animals for adverse reactions. We closely monitored the mice for signs of discomfort or distress and euthanized the animals after 3 hours when combination-treated mice exhibited reduced activity levels. We then performed tissue immunofluorescence microscopy for anti-CD31 and anti–Cl-Casp3 on liver, kidney, heart, and lung (Fig. 5, E to H). Quantification of Cl-Casp3$^+$ cells among CD31$^+$ and CD31$^-$ cells revealed a significant increase in the number of Cl-Casp3$^+$ cells in CD31$^+$ ECs in all four tissues in mice treated with combined BCL-$X_L$ and MCL-1 inhibitors, signifying rapidly induced apoptosis in these cells (Fig. 5, I to L). BCL-$X_L$ inhibition alone did not result in any increase of Cl-Casp3$^+$ ECs, while MCL-1 inhibition alone resulted in significant EC Cl-Casp3$^+$ increase in kidney, heart, and lung, although at a lower level than seen with the combination treatment. These results indicate that treatment with MCL-1 inhibitors may contribute to the development of vascular toxicities, while combination treatment with BCL-$X_L$ and MCL-1 inhibitors for cancer treatment may not be tolerable because of acute vascular toxicities. Among CD31$^-$ cells, only the lung showed a significant increase in number of Cl-Casp3$^+$ cells and only for the combined A-1331852 and S63845 treatment.

## ECs and VSMCs have different toxicity profiles in response to targeted agents

Although targeted anticancer agents can be highly effective in the clinic, many are associated with a myriad of vascular toxicities, often becoming apparent later in clinical testing or even after regulatory approval, highlighting the need for earlier detection of potential toxicities in vitro, especially in human cells (*28*). To determine whether targeted agents are toxic to vascular cells, we first measured apoptosis after 48 hours of treatment with a panel of targeted agents. Examining responses to these agents at $C_{max}$ doses, we found that while many were not toxic to vascular cells and thus not expected to cause toxicity in vivo (Fig. 6A), certain agents were toxic at $C_{max}$ doses including midostaurin and 17-DMAG (17-Dimethylaminoethylamino-17-demethoxygeldanamycin)—these agents have been previously linked to CV ADRs in patients (*29*, *30*).

We next compared apoptosis induction by proteasome inhibitors that are commonly used to treat hematologic malignancies. We found that carfilzomib was the most toxic proteasome inhibitor to vascular cells, followed by bortezomib and then ixazomib (Fig. 6B). To investigate how our results may align with clinical experiences, we again performed a disproportionality analysis for commonly reported cancer therapy–associated ADRs using the following MedDRA preferred terms: Blood pressure (BP) increased, Hypertension, Myocardial ischemia, and Myocardial infarction (Fig. 6, C and D). Our results show that ixazomib was not associated with any overrepresentation of these ADRs, while bortezomib was associated with only myocardial ischemia. In agreement with our in vitro sensitivity data, carfilzomib was most strongly associated with multiple ADRs including hypertension, myocardial ischemia, myocardial infarction, and BP increased. Notably, the relative rates of these ADRs were aligned with each agent's relative toxicity to ECs and VSMCs in vitro.

One of the most successful classes of targeted therapies are tyrosine kinase inhibitors (TKIs), which were initially developed to treat chronic myelogenous leukemia (CML) because it is driven by an oncogenic BCR-ABL1 kinase gene fusion. While imatinib (Gleevec), the first drug approved in CML, is relatively safe from a vascular standpoint, later-generation therapies such as nilotinib and ponatinib have been associated with vascular toxicities, with ponatinib having been transiently removed from the market because of these toxicities (*31*). To assess whether our system recapitulates the vascular toxicity profiles observed clinically with CML TKIs, we treated our cell panel with imatinib, bosutinib, dasatinib, nilotinib, and ponatinib and measured induction of apoptosis after 48 hours (Fig. 7A). We found that imatinib, bosutinib, and dasatinib were only mildly toxic to vascular cell types. However, nilotinib was highly toxic to VSMCs and ponatinib was highly toxic to both ECs and VSMCs.

To investigate whether the differential apoptosis induction between ECs and VSMCs by these TKIs is consistent with clinical outcomes, we queried VigiBase to find whether there is an overrepresentation of the ADR BP increased among patients with CML TKI treatments, a known side effect of certain TKIs. We found that none of the CML TKIs had statistically significant IC (i.e., $IC_{025} > 0$) or ROR (i.e., $ROR_{025} > 1$) for increased BP except ponatinib (Fig. 7A). This suggests that apoptosis of ECs (potentially in combination with VSMC apoptosis) may contribute to increased BP in CML patients treated with ponatinib but not other BCR-ABL–targeting TKIs. One major difference between ponatinib and the other CML TKIs is its inhibitory effects on vascular endothelial growth factor receptors

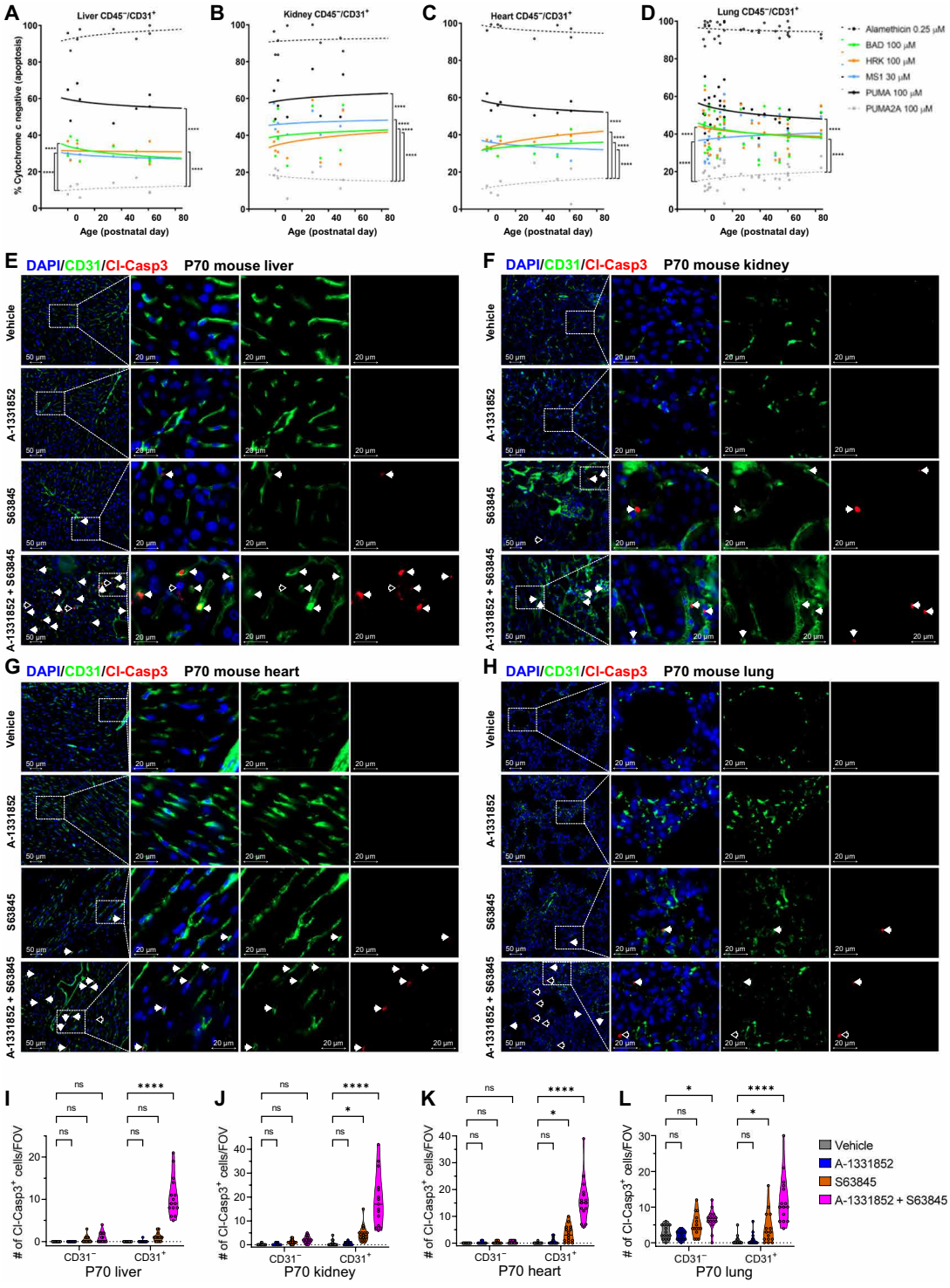


**Fig. 5. Vascular ECs in vivo are vulnerable to inhibition of prosurvival BCL-2 family proteins and undergo apoptosis in response to combined MCL-1 and BCL-$X_L$ inhibition.** (**A** to **D**) Summary BH3 profiling data for $CD45^-/CD31^+$ cells for the sensitizer BH3 peptides BAD, HRK, MS1, and PUMA in (A) liver, (B) kidney, (C) heart, and (D) lung during postnatal development. Each data point indicates data from one tissue specimen; $n = 8$ to 32. (**E** to **H**) Representative images of immunofluorescence staining for CD31 and Cl-Casp3 in (E) liver, (F) kidney, (G) heart, and (H) lung from P70 mice 3 hours after either treatment with BCL-$X_L$ inhibitor A-1331852, MCL-1 inhibitor S63845, or a combination of both. Filled arrowheads indicate examples of cells that are positive for both CD31 and Cl-Casp3; empty arrowheads indicate cells that are positive for only Cl-Casp3. $n = 3$ animals per treatment condition. (**I** to **L**) Quantification of number of Cl-$Casp3^+$ cells in $CD31^+$ or $CD31^-$ cells per 20× field of view from immunofluorescence images of control or BH3 mimetic–treated (I) liver, (J) kidney, (K) heart, and (L) lung. $n = 15$ (3 animals per treatment condition, 5 images per animal).

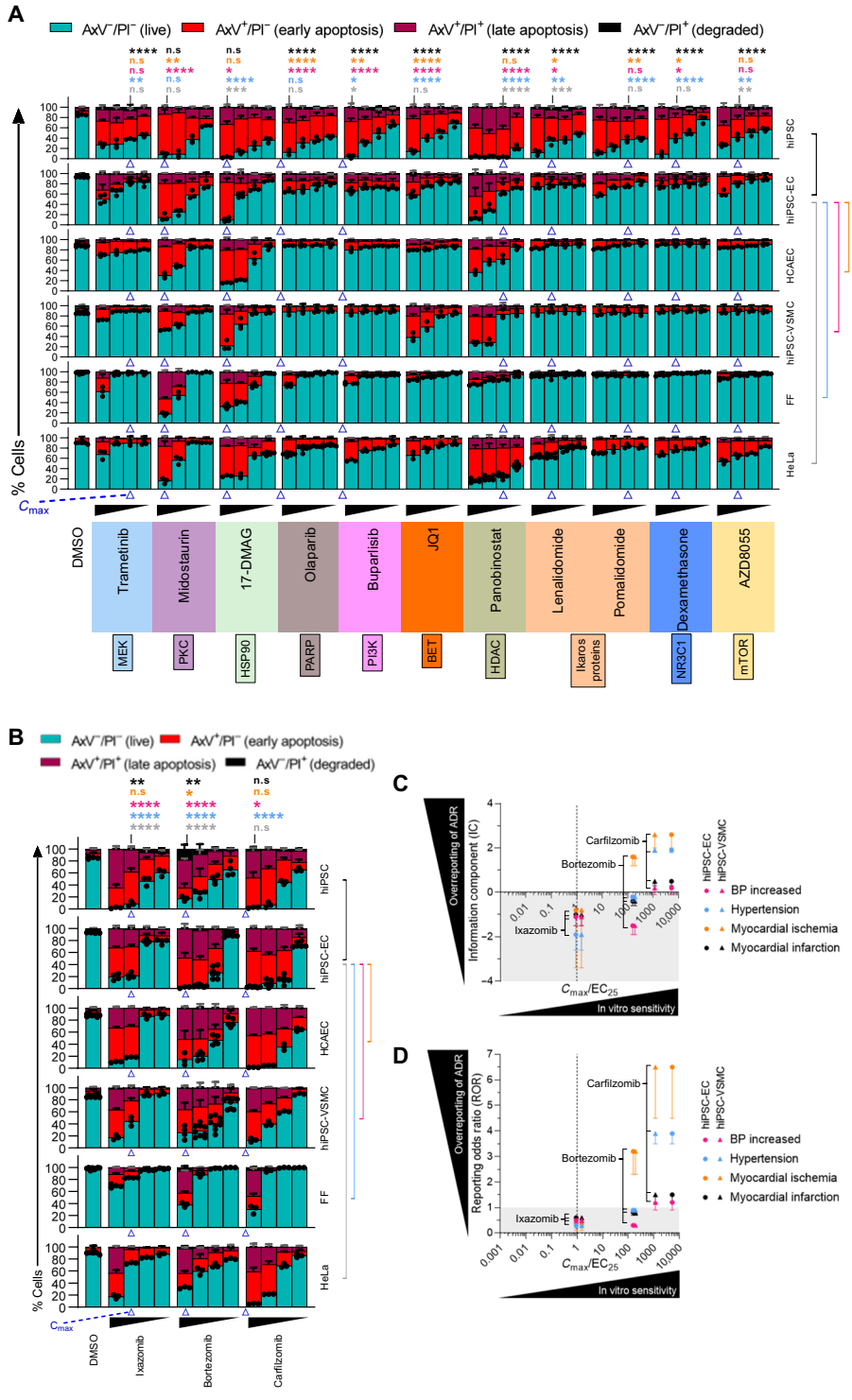


**Fig. 6. Vascular cell types have different toxicity profiles in response to targeted agents.** (**A** and **B**) AxV/PI staining of hiPSCs, hiPSC-ECs, hiPSC-VSMCs, primary HCAECs, primary human FFs, and HeLa cells 48 hours after treatment start in response to (A) a multitude of different targeted cancer therapeutics and (B) proteasome inhibitors; $n = 3$ to 9 biological replicates. $C_{max}$ arrows indicate which concentration is comparable to maximum patient plasma concentration. Significance: ns, not significant, $^{*}P < 0.05$, $^{**}P < 0.01$, $^{***}P < 0.001$, and $^{****}P < 0.0001$. (**C** and **D**) VigiBase overrepresentation of BP increased, Hypertension, Myocardial ischemia, and Myocardial infarction shown as IC (C) or ROR (D) plotted against $C_{max}/EC_{25}$ of proteasome inhibitors for hiPSC-ECs and hiPSC-VSMCs. Error bars show lower end of 95% credibility and confidence intervals ($IC_{025}$ and $ROR_{025}$), respectively. Statistical significance was set at $IC_{025} > 0$ and $ROR_{025} > 1$, respectively.

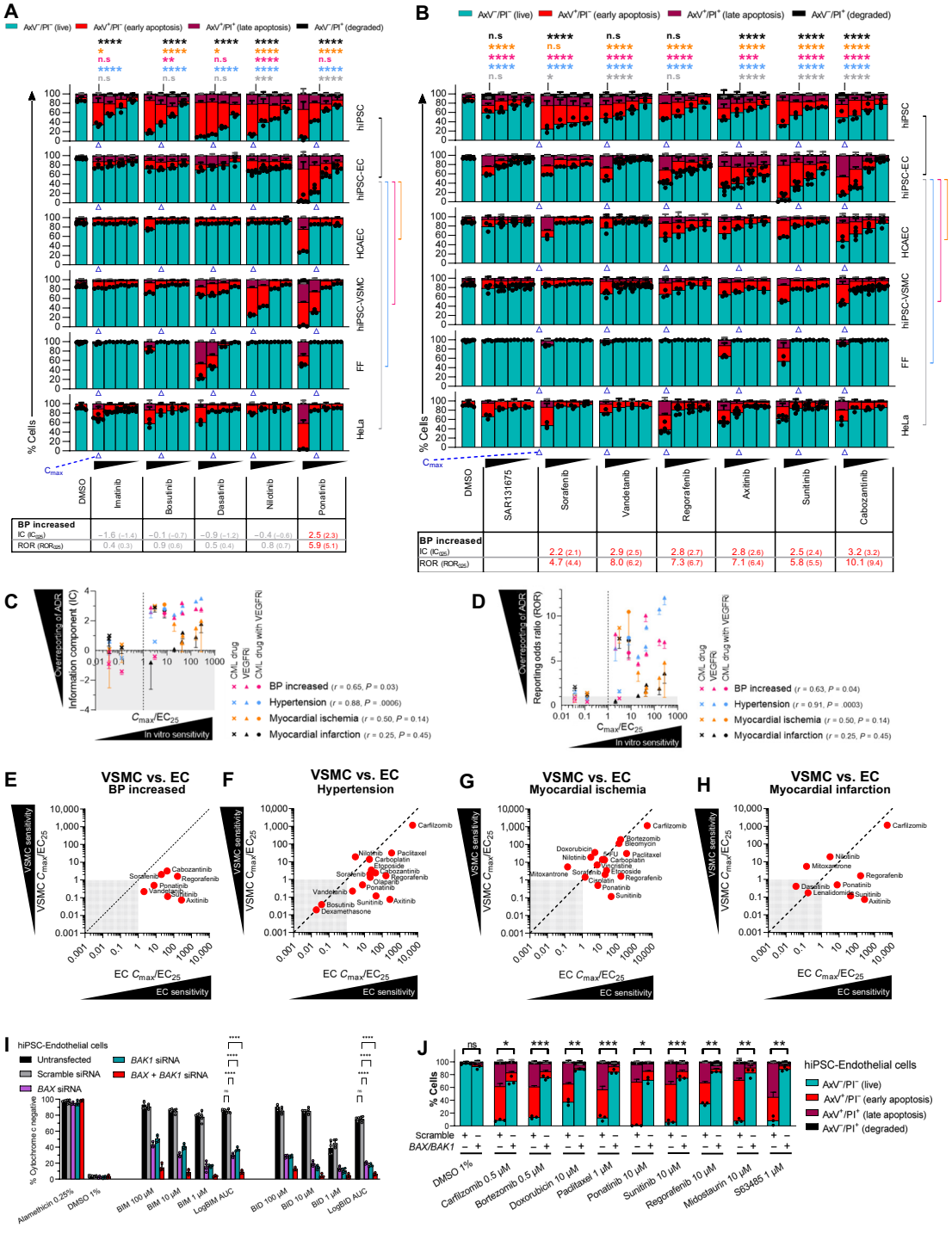


**Fig. 7. Clinical observations of drug-induced cardiovascular adverse events correspond to vascular cell type sensitivity to chemotherapeutics and targeted agents.** (**A** and **B**) AxV/PI staining of hiPSC-derived, primary human, and HeLa cells 48 hours after treatment start in response to (A) BCR-ABL–targeting CML drugs and (B) VEGFR-targeting drugs; $n = 3$ to 9 biological replicates. $C_{max}$ arrows indicate what concentration is comparable to maximum patient plasma concentration. $C_{max}$ arrows indicate which concentration is comparable to maximum patient plasma concentration. Significance: ns, not significant, $^{*}P < 0.05$, $^{**}P < 0.01$, $^{***}P < 0.001$, and $^{****}P < 0.0001$. Tables in (A) and (B) show VigiBase overrepresentation of BP increased. (**C** and **D**) VigiBase overrepresentation of BP increased, Hypertension, Myocardial ischemia, and Myocardial infarction shown as IC (C) or ROR (D) plotted against $C_{max}/EC_{25}$ of CML TKIs and VEGFR inhibitors for hiPSC-ECs. Error bars show lower end of 95% credibility and confidence intervals ($IC_{025}$ and $ROR_{025}$), respectively. (**E** to **H**) $C_{max}/EC_{25}$ for hiPSC-VSMCs versus hiPSC-ECs, for drugs with significant VigiBase overrepresentation of (E) BP increased, (F) Hypertension, (G) Myocardial ischemia, and (H) Myocardial infarction. Statistical significance was set at $IC_{025} > 0$ and $ROR_{025} > 1$, respectively [indicated by red text in (A) and (B)]. Correlation between IC or ROR and $C_{max}/EC_{25}$ was determined using Spearman's rank-order analysis. (**I**) BH3 profiling of hiPSC-ECs transfected with siRNA for *BAX*, *BAK1*, or both; $n = 4$ biological replicates. (**J**) AxV/PI staining of hiPSC-ECs transfected with *BAX* and *BAK1* siRNA and treated with different classes of cancer therapeutics for 48 hours; $n = 3$ biological replicates.

(VEGFRs) (*32*), and thus, we hypothesized that induction of apoptosis through inhibition of VEGFR could be what is causing the enhanced toxicity of ponatinib in hiPSC-ECs. To test this, we chose a number of approved TKIs that target VEGFR and other kinases and measured apoptosis induction in our panel of different cell types. These all showed higher induction of apoptosis in ECs compared with VSMCs and were all significantly associated with the ADR BP increased (Fig. 7B).

We then compared VigiBase data for BP increased, Hypertension, Myocardial ischemia, and Myocardial infarction for these TKIs and saw that drugs that potently kill ECs in vitro ($C_{max}/EC_{25} > 1$) were in general associated with more vascular toxicities (Fig. 7, C and D). A similar pattern was not seen when plotting the VigiBase data against VSMC in vitro sensitivity (fig. S6, A and B), suggesting that EC apoptosis might play a substantial role in the development of these toxicities.

### Clinical observations of drug-induced CV adverse events correspond to vascular cell type in vitro apoptosis induction

We next sought to determine whether the drugs associated with vascular toxicities in patients were more toxic to ECs or VSMCs in our in vitro assay. We therefore compared $C_{max}/EC_{25}$ for hiPSC-ECs with that of hiPSC-VSMCs for each of our drugs that had VigiBase information (table S1). We then compared the relative drug sensitivities directly between ECs and VSMCs for drugs that are significantly overrepresented for patients with increased BP, hypertension, myocardial ischemia, or myocardial infarction. We found that for increased BP and hypertension, in particular, the drugs induced more apoptosis in ECs than in VSMCs (Fig. 7, E and F). Furthermore, most of the drugs with associated toxicities show a $C_{max}/EC_{25}$ value above 1 for either cell type, indicating that the cells are dying in vitro in response to drugs at concentrations that are achieved in clinical use (Fig. 7, E to H).

Together, these observations implicate drug-induced EC apoptosis as a driver of multiple vascular toxicities, in particular, BP dysregulation, and likely other healthy tissue toxicities via vascular disruption. Further, they indicate that short-term apoptosis induction in hiPSC-derived vascular cells could be potentially used as a screening platform for long-term vascular toxicities of newly developed anticancer drugs.

### Apoptotic priming and drug sensitivity in ECs is dependent on the mitochondrial apoptosis pathway

Last, we wanted to test the extent to which blocking mitochondrial apoptosis may protect vascular cells from anticancer agent–induced cell death. We therefore knocked down *BAX* and *BAK1* separately or in combination in hiPSC-ECs and first confirmed apoptosis blockade via BH3 profiling (Fig. 7I). Our results show that knocking down either gene resulted in a blunting of apoptotic priming, which was further intensified with dual knockdown, to the point where the cells were not responsive to even the highest concentrations of BIM BH3 or BID BH3 peptide. Further, we found that *BAX*/*BAK1* dual-knockdown hiPSC-ECs were significantly less sensitive to a representative panel of cytotoxic and targeted drugs than untransfected hiPSC-ECs. Together, these results demonstrate the importance of the intrinsic pathway in mediating cell death in ECs in response to cancer therapeutics and suggest that blocking apoptosis in ECs while maintaining cancer cell death may reduce vascular toxicities in patients and thus improve outcomes.

## DISCUSSION

Recent studies have established that apoptosis is dynamically regulated in healthy tissues as part of homeostasis and plays a major role in explaining toxicities that arise as a consequence of cancer therapy (*1*, *2*, *6*, *14*, *33*–*35*). This is especially true in the pediatric setting, where young children are much more susceptible to radiotherapy-induced cognitive decline and doxorubicin-induced cardiotoxicity (*16*, *36*). However, in many healthy tissues, most cells become more resistant to apoptosis during postnatal development and some completely lose their apoptotic machinery by adulthood, rendering them resistant to apoptosis-inducing cancer therapeutics (*14*–*16*). We were surprised to find that vascular ECs retain their apoptotic priming into adulthood, even in tissues where most of the surrounding cells are unprimed or completely refractory to apoptosis. Because of this higher apoptotic sensitivity, it is likely that vascular cells are involved in initiating or driving not only vascular toxicities to cancer therapies but also toxicities in otherwise apoptosis refractory tissues. This could be mediated through a multitude of paths including loss of barrier function causing leakage and restriction of downstream blood flow leading to local oxygen deprivation, proinflammatory signaling at damaged sites leading to immune cell recruitment and chronic inflammation, or direct capillary destruction and local ischemia (*4*).

It is important to note that while BH3 profiling is an established method of measuring apoptotic priming in cancerous as well as healthy cells, it relies on measurements of cells in single-cell suspension, which could potentially alter the state of the apoptosis pathway (*7*, *9*–*14*). In an effort to counteract this, we also measured Cl-Casp3 activity in response to cytotoxic treatment in intact tissue sections using immunofluorescence staining. Further, BH3 profiling does not take into account the involvement of apoptosis regulators upstream or downstream of MOMP or modes of cell death other than intrinsic apoptosis, which can also affect cell fate (*37*–*39*).

While development of hiPSC-based screening platforms for the CV toxicity of cancer drugs has been reported previously, most research has focused on hiPSC-derived cardiomyocytes and investigation of cardiac toxicities (*17*, *18*, *40*–*43*). Using hiPSC-derived cells of the vasculature, we established a platform to measure the vascular toxic effects of various cancer therapeutics, including most standard chemotherapy drug families. It should be noted that the measurements performed here are performed in an in vitro setting and measures apoptosis induction, which can be considered a very short-term response relative to the clinical end points studied. Results from the in vitro platform should not be interpreted as directly causing the same levels of apoptosis in ECs and VSMCs in patients, or that apoptosis is the sole mechanism responsible for disease formation and progression, but rather should be interpreted as the potential involvement of apoptosis as an initiating factor in disease development and a possible early indicator of later pathologies. We found that among the cancer therapy drugs, many seemed to induce cell death in the cells of the vasculature (ECs and/or VSMCs) at doses that are normally used in in vitro settings and are directly translatable to the clinic. This may offer insight into the mechanisms by which vascular toxicities arise in cancer patients and may be prevented by inhibiting apoptosis (*4*). We also found differential toxicity profiles between ECs and VSMCs to different cancer therapeutics. For example, doxorubicin induced more apoptosis in VSMCs than in ECs (*32*, *44*, *45*). The cardiotoxic effects of doxorubicin and other anthracyclines in children are well known and are attributed to the death

of cardiomyocytes (*3*, *16*). It is possible that the death of VSMCs also contributes to this toxicity and may also drive doxorubicin-induced vascular toxicities in adults. Conversely, we found that CML-targeting TKIs have clinical toxicities that align with their effects on ECs in vitro. In particular, TKIs such as ponatinib and nilotinib are restricted in their use as second-line treatment options for CML on account of CV ADRs such as peripheral arterial disease, coronary artery disease, and acute myocardial infarction (*32*). Many studies have investigated the CV effects of proteasome inhibition, and while the current clinical recommendations are to follow the same general rules as for other cancer treatments with potential CV toxicity, there is emerging evidence advocating further cardio-oncological monitoring, especially considering carfilzomib treatment. Notably, our studies suggest that pharmacologic reduction of apoptotic sensitivity in vascular cells before administration of cancer therapies may ameliorate systemic vascular dysfunction and tissue-specific toxicities.

Our studies of in vitro EC and VSMC toxicity to cancer therapeutics also revealed a high sensitivity to BH3 mimetics, especially those inhibiting BCL-$X_L$ and MCL-1. While BCL-2 inhibitors have thus far had the most clinical success among the BH3 mimetics (mainly targeting hematological cancers including chronic lymphocytic and acute myelogenous leukemias) (*46*, *47*), there are currently a multitude of clinical trials ongoing with BCL-$X_L$ and MCL-1 inhibitors for treatment of various hematological and solid cancers (*48*, *49*). Several preclinical studies are also advocating the combination of BH3 mimetics with different BCL-2 family targets to increase antitumor effects or combining these agents with other apoptosis-inducing therapies (*14*, *48*). While some of these studies report tolerable in vivo toxicity experiments, most are only performed on a short-term basis and do not take into account the long latency period frequently associated with CV toxicity (*4*). Our results show that both ECs and VSMCs are highly sensitive to BH3 mimetic combinations targeting several prosurvival BCL-2 family members, especially combined BCL-$X_L$ and MCL-1 inhibition and, to a lesser extent, MCL-1 inhibition alone. Furthermore, the higher priming we detected in ECs from young mice as compared to adult suggests that vascular cells may die in response to anticancer agents including BH3 mimetics at higher rates than in adults. Whether this is counterbalanced by increased capacity for vascular regeneration and repair at younger ages is unknown. Last, the MCL-1 inhibitor S63845 has a sixfold higher affinity for human MCL-1 than for mouse MCL-1, indicating that potential on-target toxicities may be underestimated when using a mouse model (*50*). This may translate into potentially intractable long-term toxicities of the CV system and should be taken into account when designing clinical trials with novel BH3 mimetics. On the basis of our studies, incorporation of enhanced monitoring for potential vascular toxicities is warranted.

## MATERIALS AND METHODS

### Animal care and use

Cohorts of mice were housed and bred in a colony in accordance with the policies and regulations set forth by the Harvard T.H. Chan School of Public Health (HSPH) Institutional Animal Care and Use Committee (IACUC), under protocol 5245. All animal experiments were approved by the IACUC under HSPH protocol #IS00001059-3. C57BL/6J mice (wild type) (The Jackson Laboratory), were used for tissue collection. For whole-body irradiation experiments, mice were placed in an acrylic pie cage and irradiated with 24 Gy using a Cs-137 source (Mark 1 Irradiator, Shepherd & Associates) with a dose rate of 1.8 Gy/min. Animals were sacrificed at 6, 12, 18, or 24 hours after irradiation, and tissues were collected for downstream analysis. For BH3 mimetic treatment, animals were intravenously injected with A-1331852 (25 mg/kg) or S63845 (25 mg/kg) or a combination of A-1331852 and S63845 (25 + 25 mg/kg).

### Tissue processing

For BH3 profiling, AxV, plasma membrane integrity, and caspase-3/7 activity measurements, tissue samples from mice of different ages (P0 to P85) were dissociated into single-cell suspensions using the Papain Dissociation System (Worthington Biochemical Corporation) with a modified protocol, as previously described (*51*). Briefly, 50 to 100 g of tissue sample were roughly chopped and submerged in 500 μl of Earle's balanced salt solution (EBSS) with papain protease (20 U/ml) and 0.005% deoxyribonuclease (DNase) and incubated at 37°C with frequent agitation for 15 min. Samples were placed on ice and triturated with cut 1-ml pipette tips and were left to settle for 2 to 5 min before the cloudy cell suspension was transferred to new tubes and centrifuged at 200*g* for 5 min at 4°C. The resulting pellet was resuspended in cold EBSS with 0.005% DNase, bovine serum albumin (BSA) (1 mg/ml), and ovomucoid protease inhibitor (1 mg/ml). This suspension was layered on top of a solution of cold EBSS with BSA (10 mg/ml) and ovomucoid protease inhibitor (10 mg/ml) to create a discontinuous density gradient and then centrifuged at 72*g* for 6 min at room temperature. Supernatant was discarded, and the pellet was collected for subsequent staining and analysis.

### Cell culture

For human iPSCs, tissue culture–treated dishes were coated for 1 hour at room temperature with Geltrex (Life Technologies) reconstituted in Dulbecco's modified Eagle's medium (DMEM) medium (Corning). Human DiPS 1016 SeVA iPSC stocks (Harvard Stem Cell Institute iPS Core Facility, Harvard University) were thawed in complete StemFlex medium (Life Technologies) containing 10 μM Rho-associated, coiled coil–containing protein kinase (ROCK) inhibitor Y-27632 (Calbiochem). After 24 hours, the medium was replaced with complete StemFlex free of ROCK inhibitor. Cells were detached using Accutase (STEMCELL Technologies) and split 1:5 to 1:10 before reaching confluence; cells were cultured in complete StemFlex medium supplemented with ROCK inhibitor for the first 24 hours. All culture media were supplemented with penicillin-streptomycin (Life Technologies) and Plasmocin (InvivoGen) and changed every other day unless otherwise specified. Human FFs were collected from neonatal foreskin specimens provided by Brigham and Women's Hospital and cultured in DMEM/F-12 with 10% fetal bovine serum (FBS) (Life Technologies) and 1% penicillin-streptomycin (Life Technologies). Primary HCAECs were purchased from Lonza (CC-2585) and cultured in Endothelial Cell Growth Medium-2 Bulletkit (EGM-2) medium from Lonza (CC-3162). HeLa cells were cultured in DMEM with 10% FBS (Life Technologies) and 1% penicillin-streptomycin (Life Technologies). All cell lines were routinely tested for mycoplasma contamination and were negative throughout this study.

### Differentiation of hiPSCs

hiPSCs were differentiated as previously described (*23*). Briefly, hiPSC clones were split to 50% confluence and cultured overnight in StemFlex medium (Life Technologies) with 10 μM ROCK inhibitor.

The next day (day 1), differentiation was initiated by replacing the medium with N2B27, which consists of equal parts of Neurobasal medium and DMEM/F-12 GlutaMAX (Life Technologies) supplemented with B-27 without vitamin A (Life Technologies) and N-2 supplement (Life Technologies). For the first 3 days, 6 μM CHIR-99021 (Cayman Chemicals) and BMP4 (25 ng/ml; R&D Systems) were added daily. To generate VSMCs, medium was replaced on day 4 by N2B27 supplemented with platelet-derived growth factor–BB (PDGF-BB; 10 ng/ml; PeproTech) and activin A (2 ng/ml; PeproTech). On day 6, cells were split with trypsin-EDTA (Corning) into dishes coated with human fibronectin (Sigma-Aldrich) and maintained in Medium 231 (Life Technologies) supplemented with Smooth Muscle Growth Supplement (Life Technologies). To generate ECs, the same protocol was followed for the first 3 days to achieve the mesodermal lineage, but on day 4, the medium was replaced with N2B27 supplemented with VEGF (200 ng/ml; PeproTech) and 2 μM forskolin (Sigma-Aldrich). On day 6, cells were split and the differentiated ECs were either magnetic-activated cell sorting (MACS)–separated using CD144 MicroBeads (Miltenyi Biotec) or flow cytometry–sorted for $CD144^+$ cells to isolate the population expressing VE-cadherin. Endothelial lineage cells were maintained in EGM-2 Endothelial Cell Growth Medium (Lonza). All culture media were supplemented with penicillin-streptomycin (Life Technologies) and Plasmocin (InvivoGen) and changed every other day unless otherwise specified. Differentiation of hiPSCs into adipocytes was performed as published (*52*). Briefly, hiPSCs were passaged and grown in suspension culture to form embryoid bodies. After 1 week, the embryoid bodies were plated on tissue culture–treated plastic and grown in DMEM + 10% FBS. The outgrowing mesenchymal progenitor cells (MPCs) were used from passage 4 to 8. For adipocyte differentiation, MPCs were infected with previously described lentivirus to express the transactivator rtTA and inducible expression of PPARg2. MPCs were passaged and grown to confluence and then exposed to doxycycline (700 ng/ml) for 2 weeks in the previously established A2 medium and then 1 week without doxycycline in A2 medium and used for assays.

### siRNA knockdown experiments

HiPSC-ECs were seeded onto human collagen–coated six-well plates to perform small interfering RNA (siRNA) knockdowns. We seeded cells at 200,000 cells per well of a six-well plate and waited for 2 days to perform the siRNA knockdown with Lipofectamine RNAiMAX from Invitrogen Thermo Fisher Scientific (catalog no. 13778030). Predesigned *BAX* (assay ID 202474) and *BAK1* (assay ID 120199) siRNA were purchased from Thermo Fisher Scientific Ambion Technologies. Transfection of cells was performed according to the manufacturer's protocol. Briefly, we diluted 25 pmol of siRNA per well in Opti-MEM medium (Gibco Thermo Fisher Scientific, #31985070) and mixed this with 9 μl of Lipofectamine diluted in Opti-MEM as per the manufacturer's protocol. After a 5-min incubation, the Lipofectamine RNAiMAX with siRNA complex was added to the cells directly. EC medium (Lonza, EGM-2) was replaced 2 days after transfection with siRNA, and cells were used for assays described here 48 hours after transfection.

### BH3 profiling

Cell pellets from tissue dissociation were resuspended in 100 μl of fluorescence-activated cell sorting (FACS) stain buffer [2% FBS in phosphate-buffered saline (PBS)] with 1 μl of anti-CD31–Brilliant Violet 786 (clone 390, BD Biosciences) and 1 μl of anti-CD45–allophycocyanin (APC)/Cy7 (clone 30-F11, BioLegend). Lung and kidney single-cell suspensions also received 1 μl of anti–EPCAM–Alexa Fluor 488 (clone G8.8, BioLegend), and liver single-cell suspensions also received 1 μl of anti–GLUT2–phycoerythrin (PE) (Bioss). Cells were stained on ice for 25 min away from light and then centrifuged at 200*g* for 5 min at 4°C and subjected to flow cytometry–based BH3 profiling as previously described (*9*). In vitro cultured cells were collected, centrifuged at 200*g* for 5 min, and directly subjected to BH3 profiling. Briefly, cells were treated with activator or sensitizer BH3 peptides (New England Peptide) for 60 min at 28°C in Mannitol Experimental Buffer (MEB) [10 mM Hepes (pH 7.5), 150 mM mannitol, 50 mM KCl, 0.02 mM EGTA, 0.02 mM EDTA, 0.1% BSA, and 5 mM succinate] with 0.001% digitonin. Peptide sequences were as follows: BIM (Ac-MRPEIWIAQELRRIGDEFNA-NH2), BID (Ac-EDIIRNIARHLAQVGDSMDRY-NH2), PUMA (Ac-EQWAREIGAQLRRMADDLNA-NH2), BAD (Ac-LWAAQRYGRELRRMSDEFEGSFKGL-NH2), HRK (Ac-WSSAAQLTAARLKALGDELHQ-NH2), and MS1 (Ac-RPEIWMTQGLRRLGDEINAYYAR-NH2). Alamethicin at 0.25 μM and PUMA2A (a mutant inactive PUMA peptide, Ac-EQWAREIGAQARRMAADLNA-NH2) at 100 μM were used as positive and negative controls, respectively. After peptide exposure, cells were fixed in 2% paraformaldehyde for 15 min, followed by neutralization through the addition of neutralizing (N2) buffer [1.7 M tris base and 1.25 M glycine (pH 9.1)]. Cells were stained overnight with 4′,6-diamidino-2-phenylindole (DAPI) (1:1000t Abcam) and anti–cytochrome c–Alexa Fluor 647 (1:2000; clone 6H2.B4, BioLegend) in a saponin-based intracellular stain buffer (final concentration: 0.1% saponin and 1% BSA). Cells isolated from heart were also stained with anti–cTnT-PE in the intracellular stain buffer (1:600; clone REA400, Miltenyi Biotec). Cytochrome c release in response to BH3 peptide treatment was measured on an Attune NxT flow cytometer (Thermo Fisher Scientific). Gating (see fig. S1A) was performed to select all singlet nucleated ($DAPI^+$) events. Then, PBMCs were separated out using CD45 staining. All remaining cell identity stains were analyzed on $CD45^-$ gated cells.

For BH3 profiling of hiPSC-WAT, a JC1-based assay was used and performed on hiPSC-ECs in parallel (*14*). Briefly, BH3 peptides in MEB were deposited into a black 384-well plate, one treatment per well, in triplicate for each independent experiment. Single cells of hiPSC-EC and hiPSC-WAT were resuspended in MEB with 0.001% digitonin and mixed 1:1 with a dye solution containing digitonin and JC1 in MEB. Cells were kept at room temperature for 5 min to allow for cell permeabilization and dye equilibration. Cells were then added to each treatment well in the 384-well plate, and fluorescence at 590 nm was measured every 5 min at 32°C for a total of 120 min. Relative mitochondrial depolarization was defined as the magnitude of mitochondrial potential loss resulting from BH3 peptide treatments compared with negative control PUMA2A and positive control alamethicin.

### Cytochrome c measurements in isolated mitochondria

Liver tissue from a P86 mouse was dissociated using Dounce homogenization, and measurement of cytochrome c content in mitochondrial fractions was performed as previously described (*53*). Briefly, cells were quantified using the Vi-CELL XR Cell Viability Analyzer (Beckman Coulter), permeabilized with 0.025% digitonin in a mitochondrial resuspension buffer [100 mM sucrose (Sigma-Aldrich),

20 mM Hepes-KOH (pH 7.5; Gibco), 100 mM KCl (Sigma-Aldrich), 2.5 mM $MgCl_2$ (Sigma-Aldrich), 1× cOmplete protease inhibitors without EDTA (Roche, #04693132 001), and pepstatin A (8 μg/ml; MedChem Express)] for 10 min on ice, then separated into 50-μl aliquots containing 500,000 cells each, and treated with BH3 peptides for 30 min at 30°C. Cells were then centrifuged at 13,000*g* for 5 min at 4°C. Pellet was collected and analyzed by SDS–polyacrylamide gel electrophoresis and Western blot for anti–cytochrome c (Cell Signaling Technology, #12963).

### Western blotting

Western blotting was performed as previously described (*13*). Briefly, the polyvinylidene difluoride membrane (Bio-Rad) was incubated with the primary antibody against glyceraldehyde-3-phosphate dehydrogenase (GAPDH) (#2118, rabbit, 1:1000), MCL-1 (#94296, rabbit, 1:1000), BCL-XL (#2764, rabbit, 1:1000), BCL-2 (#2872, rabbit, 1:1000), BAX (#2772, rabbit, 1:1000), BIM (#2933, rabbit, 1:1000), PUMA (#98672, rabbit, 1:1000), and BID (#11958 , rabbit, 1:1000) from Cell Signaling Technology, BAK (#06-536, rabbit, 1:1000) from Millipore Sigma, and VE-cadherin (#50-128-96, mouse, 1:1000) from Fisher Scientific. The primary antibodies were labeled with secondary antibody ECL anti-rabbit immunoglobulin G (NA9340V, 1:4000), and protein bands were imaged using the SuperSignal Enzyme-Linked Immunosorbent Femto Maximum Sensitivity Substrate (Thermo Fisher Scientific, 37075). The iBright 1500 (Invitrogen) system was used to obtain blot images from membranes.

### Apoptosis measurements in cells isolated from irradiated tissue

Cell pellets from tissue dissociation were resuspended in 100 μl of FACS stain buffer (2% FBS in PBS) with 1 μl of anti–CD31–Brilliant Violet 786 (clone 390, BD Biosciences), 1 μl of anti–CD45–APC/Cy7 (clone 30-F11, BioLegend), 1 μl of parenchymal cell marker [anti–GLUT2-PE (Bioss), anti–EPCAM-PE (BioLegend), or anti–cTnT-PE (Miltenyi Biotec)], 0.02 μl of Alexa Fluor 647–conjugated AxV, 5 μl Zombie Violet (BioLegend), and 0.1 μl of CellEvent Caspase-3/7 Green Detection Reagent (Thermo Fisher Scientific). Cells were stained on ice for 45 min away from the light and then centrifuged at 200*g* for 5 min at 4°C, and fluorescence in different cell types was analyzed on an Attune NxT flow cytometer (Thermo Fisher Scientific).

### Immunocytochemistry and immunofluorescence microscopy

For immunocytochemistry of hiPSC-derived cells, cells were washed once with PBS and fixed in 4% paraformaldehyde for 10 min at room temperature. The cells were then blocked with 10% BSA with 0.1% Triton X-100 in PBS. Cells were incubated with primary antibody overnight with 5% BSA in PBS at 4°C. Cells were washed three times with PBS the next day and incubated with secondary antibodies and DAPI with 1% BSA in PBS for 1 hour at room temperature. Cells were then washed three times with PBS, and images were acquired using the Nikon Eclipse TI Immunofluorescence microscope. The primary antibodies used were CD31 (R&D Systems, catalog no. AF806), DAPI (Thermo Fisher Scientific, catalog no. D21490), phalloidin (Thermo Fisher Scientific, catalog no. A12379), and αSMA (Santa Cruz Biotechnology, catalog no. sc-130616).

For tissue samples from irradiated or BH3 mimetic–treated mice, tissue samples were fixed in Davidson's fixative [two parts 37% formalin, three parts 100% ethanol (Decon Labs Inc.), one part acetic acid (Fisher Chemicals), and three parts water] overnight. Samples were then washed three times with 100% ethanol, incubated in a 1:1 solution of 100% ethanol and Histo-Clear (Electron Microscopy Sciences) for 20 min at room temperature, followed by Histo-Clear for 20 min at room temperature, a 1:1 solution of paraffin (McCormick Scientific) and Histo-Clear for 20 min at 60°C, paraffin for 3 × 20 min at 60°C, and paraffin overnight at 60°C, and then embedded in paraffin blocks, and 5-μm sections were produced on a Leica RM2025 microtome. Sections were rehydrated, antigen retrieval was performed with pH 6.4 sodium citrate buffer (Vector Laboratories), and sections were placed in a 3% bleach solution [4 ml of 30% $H_2O_2$ (Sigma-Aldrich) and 0.8 ml of 1 M NaOH (Sigma-Aldrich) in 35.2 ml of PBS (Boston Bioproducts Inc.)], sandwiched between two 15,000 lux lights (AMZCOOL), and subjected to photobleaching for 1 hour. Sections were permeabilized in 0.25% PBS-T (Triton X-100–based, BioVision) and blocked with blocking buffer [5% donkey serum (Sigma-Aldrich) in 0.1% PBS-T] for 30 min. Primary antibodies against CD31 (R&D Systems, catalog no. AF806) and Cl-Casp3 (Cell Signaling Technology, #9661) were used at 1:200 dilution in blocking buffer with an overnight incubation at 4°C. Fluorophore-conjugated, species-specific secondary antibodies (Invitrogen, A11055 and A31573) were incubated for 1 hour at room temperature at 1:200 dilution in blocking buffer. Sections were then incubated with DAPI and mounted with Vectashield (Vector Laboratories). Images were captured with a Zeiss Axio-Observer Z1 inverted fluorescent microscope equipped with an Apotome.2 structured illumination optical sectioning device and an Axiocam 712 color camera. Three animals per treatment condition were used, and five 20× images were captured per animal (i.e., 15 images total per treatment condition). The images were deidentified and sorted in a randomized order, and the number of $CD31^-$/$Cl\text{-}Casp3^+$ and $CD31^+$/$Cl\text{-}Casp3^+$ cells per image was counted by a blinded operator.

### In vitro drug treatments and AxV/PI viability assay

Cells were plated at $10^4$ cells per well in 100 μl of culture medium on flat-bottom 96-well plates (Denville) and treated with the following drugs at the concentrations specified: cisplatin, 100, 10, 1, and 0.1 μM; carboplatin, 100, 10, 1, and 0.1 μM; palifosfamide, 100, 10, 1, and 0.1 μM; procarbazine, 100, 10, 1, and 0.1 μM; lomustine, 100, 10, 1, and 0.1 μM; temozolamide, 100, 10, 1, and 0.1 μM; bleomycin, 10, 1, 0.1, and 0.01 μM; mitoxantrone, 10, 1, 0.1, and 0.01 μM; doxorubicin, 10, 1, 0.1, and 0.01 μM; etoposide, 10, 1, 0.1, and 0.01 μM; topotecan, 10, 1, 0.1, and 0.01 μM; paclitaxel, 10, 1, 0.1, and 0.01 μM; vincristine, 10, 1, 0.1, and 0.01 μM; actinomycin, D (dactinomycin) 1, 0.1, 0.01, and 0.001 μM; bexarotene, 100, 10, 1, and 0.1 μM; 5-FU (fluorouracil), 100, 10, 1, and 0.1 μM; ara-C (cytarabine), 10, 1, 0.1, and 0.01 μM; methotrexate, 100, 10, 1, and 0.1 μM; pemetrexed, 100, 10, 1, and 0.1 μM; staurosporine, 1, 0.1, 0.01, and 0.001 μM; imatinib, 10, 1, 0.1, and 0.01 μM; bosutinib, 10, 1, 0.1, and 0.01 μM; dasatinib, 10, 1, 0.1, and 0.01 μM; regorafenib, 10, 1, 0.1, and 0.01 μM; axitinib, 10, 1, 0.1, and 0.01 μM; vandetanib, 10, 1, 0.1, and 0.01 μM; cabozantinib, 10, 1, 0.1, and 0.01 μM; sunitinib, 10, 1, 0.1, and 0.01 μM; SAR131675, 10, 1, 0.1, and 0.01 μM; ponatinib, 10, 1, 0.1, and 0.01 μM; nilotinib, 10, 1, 0.1, and 0.01 μM; midostaurin, 10, 1, 0.1, and 0.01 μM; sorafenib, 10, 1, 0.1, and 0.01 μM; trametinib, 10, 1, 0.1, and 0.01 μM; bortezomib, 1, 0.1, 0.01, and 0.001 μM; ixazomib, 1, 0.1, 0.01, and 0.001 μM; carfilzomib, 1, 0.1, 0.01, and 0.001 μM; bevacizumab, 1, 0.1, 0.01, and 0.001 μM; trastuzumab, 1, 0.1, 0.01, and 0.001 μM; 17-DMAG (alvespimycin), 1, 0.1, 0.01, and 0.001 μM; olaparib, 10,

1, 0.1, and 0.01 μM; buparlisib, 1, 0.1, 0.01, and 0.001 μM; JQ1, 10, 1, 0.1, and 0.01 μM; panobinostat, 10, 1, 0.1, and 0.01 μM; lenalidomide, 100, 10, 1, and 0.1 μM; pomalidomide, 100, 10, 1, and 0.1 μM; dexamethasone, 10, 1, 0.1, and 0.01 μM; AZD8055, 10, 1, 0.1, and 0.01 μM; ABT-199, 1, 0.1, and 0.01 μM; ABT-263, 1, 0.1, and 0.01 μM; A-1331852, 1, 0.1, and 0.01 μM; and S63845, 1, 0.1, and 0.01 μM. Combination BH3 mimetic treatment doses were 1 + 1, 0.1 + 0.1, or 0.01 + 0.01 μM for all combinations used, and all combination treatments were performed with simultaneous administration. $C_{max}$ levels for each drug (when applicable) were obtained from the literature (*54*–*71*). IR treatment at 4, 8, 12, and 16 Gy was performed using a Cs-137 source (Mark 1 Irradiator, Shepherd & Associates) with a dose rate of 1.8 Gy/min. Dimethyl sulfoxide (1%) was used as negative treatment control. After 24, 48, or 72 hours under standard tissue culture conditions, the medium was collected and moved to a fresh 96-well V-bottom plate (Greiner BioOne). Twenty-five microliters of 0.0025% trypsin (Gibco) was added to each well on the original plate and allowed to incubate for 5 min, and then trypsinized cells were added back to the medium on the V-bottom plate and stained with viability markers AxV and PI using the following protocol. A staining solution was prepared with 10× annexin binding buffer [0.1 M Hepes (pH 7.4), 1.4 M NaCl, and 25 mM $CaCl_2$ solution, sterile-filtered] and AxV/PI. Alexa Fluor 647–conjugated AxV and PI (Abcam) were added to solution at a dilution of 1:500. The staining solution was then added to the cells in solution at 1:10 dilution, and the cells were allowed to stain for 20 min on ice in the dark. AxV/PI positivity was then measured on an Attune NxT flow cytometer equipped with an autosampler (Thermo Fisher Scientific).

### Gene expression data collection and analysis

RNA was extracted from hiPSC-derived cells using the QIAcube and the RNeasy Plus Mini Kit (QIAGEN). RNA quality was ascertained with the TapeStation (Agilent), and only samples with a RNA integrity number (RIN) > 9.0 were used for sequencing. Sequencing libraries were made with a PrepX DNA library kit (Takara Bio) using an Apollo system (Takara Bio). Quality control for the libraries was performed using the KAPA library quantification kit (Roche) and the TapeStation (Agilent). Sequencing libraries were barcoded, pooled, and sequenced on HiSeq 2500 (Illumina) with single-end 150–base pair reads. Sequencing output was demultiplexed, barcodes were removed and trimmed for quality, and FastQC was run on all files for quality control. Reads were aligned to human genome assembly GRCh38 using STAR (*72*). Gene expression data from this study were deposited in National Center for Biotechnology Information's (NCBI) Gene Expression Omnibus (GEO accession GSE188240).

For mined gene expression data, Smart-Seq2 RNA-seq libraries of fluorescence-activated cell-sorted single cells in adult mice (https://doi.org/10.6084/m9.figshare.5821263.v3) and corresponding cell annotations (https://github.com/czbiohub/tabula-muris) were obtained from the Tabula Muris database (*20*). EC gene expression from embryonic mice (GSE79306) (*22*) and an additional set of adult mice (GSE95401) (*21*) was processed using Genevestigator.

Bioinformatics processing and analysis were performed in the R statistical computing environment (http://r-project.org, version 4.1.0) using Seurat v3 (*73*). Cells with <500 detected genes and <50,000 confidentially mapped reads were excluded from downstream analysis. Raw counts were converted to log counts per million by log normalization and subsequently scaled. The effects of confounding factors, including ribosomal RNA, total number of reads, and percentage of External RNA Controls Consortium controls, were removed by linear regression. Heatmaps were created using the ComplexHeatmap package (*74*), and clusters were split into slices by *k*-means partitioning.

### VigiBase analysis

A disproportionality analysis was performed as previously described (*25*). Briefly, VigiBase allows for case/noncase analysis (disproportionality analysis), which we used to study whether suspected drug-induced CV events were differentially reported with a specific drug compared with CV events reported in the entire database with all other drugs. Disproportionality analysis compares the proportion of selected specific ADRs reported for a single or a group of drugs (e.g., ponatinib) with the proportion of the same ADR for a control group of drugs (e.g., entire database). The denominator in these analyses is the overall ADR reported for each group of drugs. If the proportion of an ADR is greater in patients exposed to a group of drugs (cases) than in patients not exposed to this drug group (noncases), this suggests an association between the specific drug and the reaction and is a potential signal for safety. Disproportionality can be calculated by either the IC (a Bayesian statistic) or ROR (a Frequentist statistic) when using the entire database as comparator. Calculation of the IC using a Bayesian confidence propagation neural network was developed and validated by the Uppsala Monitoring Centre as a flexible, automated indicator value for disproportionate reporting (*75*). Probabilistic reasoning in intelligent systems (information theory) has proven to be effective for the management of large datasets, is robust in handling incomplete data, and can be used with complex variables. The information theory tool is ideal for finding drug-ADR combinations with other variables that are highly associated compared with the generality of the stored data (*75*). Several examples of validation with the IC exist, showing the power of the technique to find signals sooner after drug approval than by a regulatory agency (e.g., an association between captopril and coughing) and to avoid false positives, whereby an association between a common drug and a common ADR occurs in the database only because the drug is widely used and the ADR is frequently reported (e.g., between atorvastatin and rash) (*75*, *76*). Furthermore, we have recently published several studies using VigiBase and disproportional reporting calculation to characterize and identify new drug-ADR–associated signals, which were subsequently corroborated by preclinical mechanistic studies or prospective cohorts (*25*, *77*, *78*).

The statistical formula is as follows

$$\mathrm{IC} = \log_2\left[\left(N_{\mathrm{observed}} + 0.5\right)/\left(N_{\mathrm{expected}} + 0.5\right)\right]$$

where

$$N_{\mathrm{expected}} = \left[\left(N_{\mathrm{drug}} \times N_{\mathrm{reaction}}\right)/N_{\mathrm{total}}\right]$$

$N_{\mathrm{expected}}$ is the number of case reports expected for the drug-ADR combination. This number is computed from $N_{\mathrm{drug}}$, $N_{\mathrm{reaction}}$, and $N_{\mathrm{total}}$. $N_{\mathrm{observed}}$ is the actual number of case reports for the drug-ADR combination. $N_{\mathrm{drug}}$ is the number of case reports for the drug, regardless of ADR. $N_{\mathrm{reaction}}$ is the number of case reports for the ADR, regardless of drug. $N_{\mathrm{total}}$ is the total number of case reports in the database.

The IC is an estimate of disproportionality analyses. It is considered significant if its lower bound of the 95% credibility interval, $IC_{025}$, is greater than zero.

The MedDRA v24.0 preferred terms queried as a function of selected anticancer drugs in this analysis were "Blood pressure increased," "Hypertension," "Myocardial ischemia," and "Myocardial infarction." The VigiBase database used for analyses was dated 8 August 2021. The VigiBase database is publicly available upon request to UMC (https://who-umc.org/vigibase/).

## SUPPLEMENTARY MATERIALS

Supplementary material for this article is available at https://science.org/doi/10.1126/sciadv.abn6579

View/request a protocol for this paper from *Bio-protocol*.

## REFERENCES AND NOTES


1. S. H. Kaufmann, W. C. Earnshaw, Induction of apoptosis by cancer chemotherapy. *Exp. Cell Res.* **256**, 42–49 (2000).
2. K. A. Sarosiek, T. N. Chonghaile, A. Letai, Mitochondria: Gatekeepers of response to chemotherapy. *Trends Cell Biol.* **23**, 612–619 (2013).
3. S. E. Lipshultz, V. I. Franco, T. L. Miller, S. D. Colan, S. E. Sallan, Cardiovascular disease in adult survivors of childhood cancer. *Annu. Rev. Med.* **66**, 161–176 (2015).
4. J. Spetz, J. Moslehi, K. Sarosiek, Radiation-induced cardiovascular toxicity: Mechanisms, prevention, and treatment. *Curr. Treat. Options Cardiovasc. Med.* **20**, 31 (2018).
5. M. Santoni, F. Guerra, A. Conti, A. Lucarelli, S. Rinaldi, L. Belvederesi, A. Capucci, R. Berardi, Incidence and risk of cardiotoxicity in cancer patients treated with targeted therapies. *Cancer Treat. Rev.* **59**, 123–131 (2017).
6. R. W. Johnstone, A. A. Ruefli, S. W. Lowe, Apoptosis: A link between cancer genetics and chemotherapy. *Cell* **108**, 153–164 (2002).
7. T. Ni Chonghaile, K. A. Sarosiek, T.-T. Vo, J. A. Ryan, A. Tammareddi, V. D. G. Moore, J. Deng, K. C. Anderson, P. Richardson, Y.-T. Tai, C. S. Mitsiades, U. A. Matulonis, R. Drapkin, R. Stone, D. J. Deangelo, D. J. McConkey, S. E. Sallan, L. Silverman, M. S. Hirsch, D. R. Carrasco, A. Letai, Pretreatment mitochondrial priming correlates with clinical response to cytotoxic chemotherapy. *Science* **334**, 1129–1133 (2011).
8. M. C. Wei, W. X. Zong, E. H. Cheng, T. Lindsten, V. Panoutsakopoulou, A. J. Ross, K. A. Roth, G. R. MacGregor, C. B. Thompson, S. J. Korsmeyer, Proapoptotic BAX and BAK: A requisite gateway to mitochondrial dysfunction and death. *Science* **292**, 727–730 (2001).
9. C. Fraser, J. Ryan, K. Sarosiek, BH3 profiling: A functional assay to measure apoptotic priming and dependencies, in *BCL-2 Family Proteins. Methods in Molecular Biology*, E. Gavathiotis, Ed. (Humana Press, 2019), vol. 1877, pp. 61–76.
10. K. A. Sarosiek, X. Chi, J. A. Bachman, J. J. Sims, J. Montero, L. Patel, A. Flanagan, D. W. Andrews, P. Sorger, A. Letai, BID preferentially activates BAK while BIM preferentially activates BAX, affecting chemotherapy response. *Mol. Cell* **51**, 751–765 (2013).
11. V. Nangia, F. M. Siddiqui, S. Caenepeel, D. Timonina, S. J. Bilton, N. Phan, M. Gomez-Caraballo, H. L. Archibald, C. Li, C. Fraser, D. Rigas, K. Vajda, L. A. Ferris, M. Lanuti, C. D. Wright, K. A. Raskin, D. P. Cahill, J. H. Shin, C. Keyes, L. V. Sequist, Z. Piotrowska, A. F. Farago, C. G. Azzoli, J. F. Gainor, K. A. Sarosiek, S. P. Brown, A. Coxon, C. H. Benes, P. E. Hughes, A. N. Hata, Exploiting MCL1 dependency with combination MEK + MCL1 inhibitors leads to induction of apoptosis and tumor regression in KRAS-mutant non–small cell lung cancer. *Cancer Discov.* **8**, 1598–1613 (2018).
12. J. Crombie, C. Lossos, K. Sarosiek, A. L. Christie, C. Fraser, S. Bhatt, J. Deng, M. S. Davids, D. M. Weinstock, A. Letai, Dynamic BH3 profiling reveals novel therapeutic strategies for the treatment of double-hit lymphoma. *Blood* **130**, 2764 (2017).
13. J. Montero, K. A. Sarosiek, J. D. Deangelo, O. Maertens, J. Ryan, D. Ercan, H. Piao, N. S. Horowitz, R. S. Berkowitz, U. Matulonis, P. A. Jänne, P. C. Amrein, K. Cichowski, R. Drapkin, A. Letai, Drug-induced death signaling strategy rapidly predicts cancer response to chemotherapy. *Cell* **160**, 977–989 (2015).
14. K. A. Sarosiek, C. Fraser, N. Muthalagu, P. D. Bhola, W. Chang, S. K. McBrayer, A. Cantlon, S. Fisch, G. Golomb-Mello, J. A. Ryan, J. Deng, B. Jian, C. Corbett, M. Goldenberg, J. R. Madsen, R. Liao, D. Walsh, J. Sedivy, D. J. Murphy, D. R. Carrasco, S. Robinson, J. Moslehi, A. Letai, Developmental regulation of mitochondrial apoptosis by c-Myc governs age- and tissue-specific sensitivity to cancer therapeutics. *Cancer Cell* **31**, 142–156 (2017).
15. P. Patel, J. Karch, Regulation of cell death in the cardiovascular system. *Int. Rev. Cell Mol. Biol.* **353**, 153–209 (2020).
16. K. K. Hutchins, H. Siddeek, V. I. Franco, S. E. Lipshultz, Prevention of cardiotoxicity among survivors of childhood cancer. *Br. J. Clin. Pharmacol.* **83**, 455–465 (2017).
17. P. Liang, F. Lan, A. S. Lee, T. Gong, V. Sanchez-Freire, Y. Wang, S. Diecke, K. Sallam, J. W. Knowles, P. J. Wang, P. K. Nguyen, D. M. Bers, R. C. Robbins, J. C. Wu, Drug screening using a library of human induced pluripotent stem cell-derived cardiomyocytes reveals disease-specific patterns of cardiotoxicity. *Circulation* **127**, 1677–1691 (2013).
18. P. W. Burridge, Y. F. Li, E. Matsa, H. Wu, S.-G. Ong, A. Sharma, A. Holmström, A. C. Chang, M. J. Coronado, A. D. Ebert, J. W. Knowles, M. L. Telli, R. M. Witteles, H. M. Blau, D. Bernstein, R. B. Altman, J. C. Wu, Human induced pluripotent stem cell-derived cardiomyocytes recapitulate the predilection of breast cancer patients to doxorubicin-induced cardiotoxicity. *Nat. Med.* **22**, 547–556 (2016).
19. J. Spetz, A. G. Presser, K. A. Sarosiek, T cells and regulated cell death: Kill or be killed. *Int. Rev. Cell Mol. Biol.* **342**, 27-71 (2019).
20. The Tabula Muris Consortium, A single-cell transcriptomic atlas characterizes ageing tissues in the mouse. *Nature* **583**, 590–595 (2020).
21. R. N. Munji, A. L. Soung, G. A. Weiner, F. Sohet, B. D. Semple, A. Trivedi, K. Gimlin, M. Kotoda, M. Korai, S. Aydin, A. Batugal, A. C. Cabangcala, P. G. Schupp, M. C. Oldham, T. Hashimoto, L. J. Noble-Haeusslein, R. Daneman, Profiling the mouse brain endothelial transcriptome in health and disease models reveals a core blood-brain barrier dysfunction module. *Nat. Neurosci.* **22**, 1892–1902 (2019).
22. M. Hupe, M. X. Li, S. Kneitz, D. Davydova, C. Yokota, J. Kele, B. Hot, J. M. Stenman, M. Gessler, Gene expression profiles of brain endothelial cells during embryonic development at bulk and single-cell levels. *Sci. Signal.* **10**, eaag2476 (2017).
23. C. Patsch, L. Challet-Meylan, E. C. Thoma, E. Urich, T. Heckel, J. F. O'Sullivan, S. J. Grainger, F. G. Kapp, L. Sun, K. Christensen, Y. Xia, M. H. C. Florido, W. He, W. Pan, M. Prummer, C. R. Warren, R. Jakob-Roetne, U. Certa, R. Jagasia, P. O. Freskgard, I. Adatto, D. Kling, P. Huang, L. I. Zon, E. L. Chaikof, R. E. Gerszten, M. Graf, R. Iacone, C. A. Cowan, Generation of vascular endothelial and smooth muscle cells from human pluripotent stem cells. *Nat. Cell Biol.* **17**, 994–1003 (2015).
24. M. Lindquist, VigiBase, the WHO global ICSR database system: Basic facts. *Drug Inf. J.* **42**, 409–419 (2008).
25. J.-E. Salem, A. Manouchehri, M. Moey, B. Lebrun-Vignes, L. Bastarache, A. Pariente, A. Gobert, J.-P. Spano, J. M. Balko, M. P. Bonaca, D. M. Roden, D. B. Johnson, J. J. Moslehi, Cardiovascular toxicities associated with immune checkpoint inhibitors: An observational, retrospective, pharmacovigilance study. *Lancet Oncol.* **19**, 1579–1589 (2018).
26. J.-E. Salem, L. S. Nguyen, J. J. Moslehi, S. Ederhy, B. Lebrun-Vignes, D. M. Roden, C. Funck-Brentano, P. Gougis, Anticancer drug-induced life-threatening ventricular arrhythmias: A World Health Organization pharmacovigilance study. *Eur. Heart J.* **42**, 3915–3928 (2021).
27. S. F. Abdul Rahman, K. Muniandy, Y. K. Soo, E. Y. H. Tiew, K. X. Tan, T. E. Bates, N. Mohana-Kumaran, Co-inhibition of BCL-XL and MCL-1 with selective BCL-2 family inhibitors enhances cytotoxicity of cervical cancer cell lines. *Biochem. Biophys. Rep.* **22**, 100756 (2020).
28. J. J. Moslehi, Cardiovascular toxic effects of targeted cancer therapies. *N. Engl. J. Med.* **375**, 1457–1467 (2016).
29. E. S. Wang, J. Baron, Management of toxicities associated with targeted therapies for acute myeloid leukemia: When to push through and when to stop. *Hematology Am. Soc. Hematol. Educ. Program* **2020**, 57–66 (2020).
30. J. E. Lancet, I. Gojo, M. Burton, M. Quinn, S. M. Tighe, K. Kersey, Z. Zhong, M. X. Albitar, K. Bhalla, A. L. Hannah, M. R. Baer, Phase I study of the heat shock protein 90 inhibitor alvespimycin (KOS-1022, 17-DMAG) administered intravenously twice weekly to patients with acute myeloid leukemia. *Leukemia* **24**, 699–705 (2010).
31. J. D. Groarke, S. Cheng, J. Moslehi, Cancer-drug discovery and cardiovascular surveillance. *N. Engl. J. Med.* **369**, 1779–1781 (2013).
32. J. J. Moslehi, M. Deininger, Tyrosine kinase inhibitor-associated cardiovascular toxicity in chronic myeloid leukemia. *J. Clin. Oncol.* **33**, 4210–4218 (2015).
33. K. Nakaya, T. Hasegawa, J. Flickinger, D. Kondziolka, W. Fellows-Mayle, G. Gobbel, Sensitivity to radiation-induced apoptosis and neuron loss declines rapidly in the postnatal mouse neocortex. *Int. J. Radiat. Biol.* **81**, 545–554 (2005).
34. A. C. Paulino, L. S. Constine, P. Rubin, J. P. Williams, Normal tissue development, homeostasis, senescence, and the sensitivity to radiation injury across the age spectrum. *Semin. Radiat. Oncol.* **20**, 12–20 (2010).
35. R. Singh, A. Letai, K. Sarosiek, Regulation of apoptosis in health and disease: The balancing act of BCL-2 family proteins. *Nat. Rev. Mol. Cell Biol.* **20**, 175–193 (2019).
36. P. K. Duffner, Risk factors for cognitive decline in children treated for brain tumors. *Eur. J. Paediatr. Neurol.* **14**, 106–115 (2010).
37. S. J. Martin, C. M. Henry, S. P. Cullen, A perspective on mammalian caspases as positive and negative regulators of inflammation. *Mol. Cell* **46**, 387–397 (2012).
38. S. Fulda, K.-M. Debatin, Extrinsic versus intrinsic apoptosis pathways in anticancer chemotherapy. *Oncogene* **25**, 4798–4811 (2006).
39. T. A. Holly, A. Drincic, Y. Byun, S. Nakamura, K. Harris, F. J. Klocke, V. L. Cryns, Caspase inhibition reduces myocyte cell death induced by myocardial ischemia and reperfusion in vivo. *J. Mol. Cell. Cardiol.* **31**, 1709–1715 (1999).

40. E. G. Navarrete, P. Liang, F. Lan, V. Sanchez-Freire, C. Simmons, T. Gong, A. Sharma, P. W. Burridge, B. Patlolla, A. S. Lee, H. Wu, R. E. Beygui, S. M. Wu, R. C. Robbins, D. M. Bers, J. C. Wu, Screening drug-induced arrhythmia [corrected] using human induced pluripotent stem cell-derived cardiomyocytes and low-impedance microelectrode arrays. *Circulation* **128**, S3–S13 (2013).
41. A. Sharma, W. L. McKeithan, R. Serrano, T. Kitani, P. W. Burridge, J. C. del Álamo, M. Mercola, J. C. Wu, Use of human induced pluripotent stem cell–derived cardiomyocytes to assess drug cardiotoxicity. *Nat. Protoc.* **13**, 3018–3041 (2018).
42. F. Stillitano, J. Hansen, C. W. Kong, I. Karakikes, C. Funck-Brentano, L. Geng, S. Scott, S. Reynier, M. Wu, Y. Valogne, C. Desseaux, J. E. Salem, D. Jeziorowska, N. Zahr, R. Li, R. Iyengar, R. J. Hajjar, J. S. Hulot, Modeling susceptibility to drug-induced long QT with a panel of subject-specific induced pluripotent stem cells. *eLife* **6**, e19406 (2017).
43. M. L. Rasmussen, N. Taneja, A. C. Neininger, L. Wang, G. L. Robertson, S. N. Riffle, L. Shi, B. C. Knollmann, D. T. Burnette, V. Gama, MCL-1 inhibition by selective BH3 mimetics disrupts mitochondrial dynamics causing loss of viability and functionality of human cardiomyocytes. *iScience* **23**, 101015 (2020).
44. A. K. Pandey, E. K. Singhi, J. P. Arroyo, T. A. Ikizler, E. R. Gould, J. Brown, J. A. Beckman, D. G. Harrison, J. Moslehi, Mechanisms of VEGF (vascular endothelial growth factor) inhibitor-associated hypertension and vascular disease. *Hypertension* **71**, E1–E8 (2018).
45. P. Gougis, J. Wassermann, J. P. Spano, N. Keynan, C. Funck-Brentano, J. E. Salem, Clinical pharmacology of anti-angiogenic drugs in oncology. *Crit. Rev. Oncol. Hematol.* **119**, 75–93 (2017).
46. A. W. Roberts, M. S. Davids, J. M. Pagel, B. S. Kahl, S. D. Puvvada, J. F. Gerecitano, T. J. Kipps, M. A. Anderson, J. R. Brown, L. Gressick, S. Wong, M. Dunbar, M. Zhu, M. B. Desai, E. Cerri, S. Heitner Enschede, R. A. Humerickhouse, W. G. Wierda, J. F. Seymour, Targeting BCL2 with venetoclax in relapsed chronic lymphocytic leukemia. *N. Engl. J. Med.* **374**, 311–322 (2016).
47. R. Thijssen, A. W. Roberts, Venetoclax in lymphoid malignancies: New insights, more to learn. *Cancer Cell* **36**, 341–343 (2019).
48. N. V. Pervushin, V. V. Senichkin, B. Zhivotovsky, G. S. Kopeina, Mcl-1 as a "barrier" in cancer treatment: Can we target it now? *Int. Rev. Cell Mol. Biol.* **351**, 23–55 (2020).
49. K. A. Sarosiek, A. Letai, Directly targeting the mitochondrial pathway of apoptosis for cancer therapy using BH3 mimetics—Recent successes, current challenges and future promise. *FEBS J.* **283**, 3523–3533 (2016).
50. A. Kotschy, Z. Szlavik, J. Murray, J. Davidson, A. L. Maragno, G. le Toumelin-Braizat, M. Chanrion, G. L. Kelly, J.-N. Gong, D. M. Moujalled, A. Bruno, M. Csekei, A. Paczal, Z. B. Szabo, S. Sipos, G. Radics, A. Proszenyak, B. Balint, L. Ondi, G. Blasko, A. Robertson, A. Surgenor, P. Dokurno, I. Chen, N. Matassova, J. Smith, C. Pedder, C. Graham, A. Studeny, G. Lysiak-Auvity, A.-M. Girard, F. Gravé, D. Segal, C. D. Riffkin, G. Pomilio, L. C. A. Galbraith, B. J. Aubrey, M. S. Brennan, M. J. Herold, C. Chang, G. Guasconi, N. Cauquil, F. Melchiore, N. Guigal-Stephan, B. Lockhart, F. Colland, J. A. Hickman, A. W. Roberts, D. C. S. Huang, A. H. Wei, A. Strasser, G. Lessene, O. Geneste, The MCL1 inhibitor S63845 is tolerable and effective in diverse cancer models. *Nature* **538**, 477–482 (2016).
51. Z. Inde, B. A. Croker, C. Yapp, G. N. Joshi, J. Spetz, C. Fraser, X. Qin, L. Xu, B. Deskin, E. Ghelfi, G. Webb, A. F. Carlin, Y. P. Zhu, S. L. Leibel, A. F. Garretson, A. E. Clark, J. M. Duran, V. Pretorius, L. E. Crotty-Alexander, C. Li, J. C. Lee, C. Sodhi, D. J. Hackam, X. Sun, A. N. Hata, L. Kobzik, J. Miller, J. A. Park, D. Brownfield, H. Jia, K. A. Sarosiek, Age-dependent regulation of SARS-CoV-2 cell entry genes and cell death programs correlates with COVID-19 severity. *Sci. Adv.* **7**, eabf8609 (2021).
52. T. Ahfeldt, R. T. Schinzel, Y.-K. Lee, D. Hendrickson, A. Kaplan, D. H. Lum, R. Camahort, F. Xia, J. Shay, E. P. Rhee, C. B. Clish, R. C. Deo, T. Shen, F. H. Lau, A. Cowley, G. Mowrer, H. Al-Siddiqi, M. Nahrendorf, K. Musunuru, R. E. Gerszten, J. L. Rinn, C. A. Cowan, Programming human pluripotent stem cells into white and brown adipocytes. *Nat. Cell Biol.* **14**, 209–219 (2012).
53. S. Iyer, R. T. Uren, R. M. Kluck, Probing BAK and BAX activation and pore assembly with cytochrome c release, limited proteolysis, and oxidant-induced linkage. *Methods Mol. Biol.* **1877**, 201–216 (2019).
54. C. Tse, A. R. Shoemaker, J. Adickes, M. G. Anderson, J. Chen, S. Jin, E. F. Johnson, K. C. Marsh, M. J. Mitten, P. Nimmer, L. Roberts, S. K. Tahir, Y. Xiao, X. Yang, H. Zhang, S. Fesik, S. H. Rosenberg, S. W. Elmore, ABT-263: A potent and orally bioavailable Bcl-2 family inhibitor. *Cancer Res.* **68**, 3421–3428 (2008).
55. S. Kummar, M. E. Gutierrez, E. R. Gardner, X. Chen, W. D. Figg, M. Zajac-Kaye, M. Chen, S. M. Steinberg, C. A. Muir, M. A. Yancey, Y. R. Horneffer, L. Juwara, G. Melillo, S. P. Ivy, M. Merino, L. Neckers, P. S. Steeg, B. A. Conley, G. Giaccone, J. H. Doroshow, A. J. Murgo, Phase I trial of 17-dimethylaminoethylamino-17-demethoxygeldanamycin (17-DMAG), a heat-shock protein inhibitor, administered twice weekly in patients with advanced malignancies. *Eur. J. Cancer* **46**, 340–347 (2010).
56. G. Bocci, R. Danesi, A. di Paolo, F. Innocenti, G. Allegrini, A. Falcone, A. Melosi, M. Battistoni, G. Barsanti, P. F. Conte, M. Del Tacca, Comparative pharmacokinetic analysis of 5-fluorouracil and its major metabolite 5-fluoro-5,6-dihydrouracil after conventional and reduced test dose in cancer patients. *Clin. Cancer Res.* **6**, 3032–3037 (2000).
57. I. Gionfriddo, L. Brunetti, F. Mezzasoma, F. Milano, V. Cardinali, R. Ranieri, A. Venanzi, S. Pierangeli, C. Vetro, G. Spinozzi, E. Dorillo, H. C. Wu, C. Berthier, R. Ciurnelli, M. J. Griffin, C. E. Jennings, E. Tiacci, P. Sportoletti, F. Falzetti, H. De Thé, G. J. Veal, M. P. Martelli, B. Falini, Dactinomycin induces complete remission associated with nucleolar stress response in relapsed/refractory *NPM1*-mutated AML. *Leukemia* **35**, 2552–2562 (2021).
58. H. Tsutsumi, T. Kumakawa, M. Hirai, M. Kikukawa, Y. Arie, M. Mori, H. Kodo, N. Nakamura, Y. Murai, R. Mizutani, Plasma concentration of cytosine arabinoside (Ara-C) in the elderly patients with hematological malignancy treated by Ara-C or cytarabine ocfosfate (SPAC). *Nihon Ronen Igakkai Zasshi* **32**, 190–194 (1995).
59. S. M. C. Spoorenberg, V. H. M. Deneer, J. C. Grutters, A. E. Pulles, G. P. Voorn, G. T. Rijkers, W. J. W. Bos, E. M. W. van de Garde, Pharmacokinetics of oral vs. intravenous dexamethasone in patients hospitalized with community-acquired pneumonia. *Br. J. Clin. Pharmacol.* **78**, 78–83 (2014).
60. L. Zhuang, J. Gao, Y. Zeng, F. Yu, B. Zhang, M. Li, H. Derendorf, C. Liu, HPLC method validation for the quantification of lomustine to study pharmacokinetics of thermosensitive liposome-encapsulated lomustine containing iohexol for CT imaging in C6 glioma rats. *Eur. J. Drug Metab. Pharmacokinet.* **36**, 61–69 (2011).
61. H. He, P. Tran, H. Gu, V. Tedesco, J. Zhang, W. Lin, E. Gatlik, K. Klein, T. Heimbach, Midostaurin, a novel protein kinase inhibitor for the treatment of acute myelogenous leukemia: Insights from human absorption, metabolism, and excretion studies of a BDDCS II drug. *Drug Metab. Dispos.* **45**, 540–555 (2017).
62. L. Xiao, J.-E. Salem, S. Clauss, A. Hanley, A. Bapat, M. Hulsmans, Y. Iwamoto, G. Wojtkiewicz, M. Cetinbas, M. J. Schloss, J. Tedeschi, B. Lebrun-Vignes, A. Lundby, R. I. Sadreyev, J. Moslehi, M. Nahrendorf, P. T. Ellinor, D. J. Milan, Ibrutinib-mediated atrial fibrillation attributable to inhibition of C-terminal Src kinase. *Circulation* **142**, 2443–2455 (2020).
63. L. Markasz, G. Stuber, E. Flaberg, Å. G. Jernberg, S. Eksborg, E. Olah, H. Skribek, L. Szekely, Cytotoxic drug sensitivity of Epstein-Barr virus transformed lymphoblastoid B-cells. *BMC Cancer* **6**, 1–12 (2006).
64. D. R. Liston, M. Davis, Clinically relevant concentrations of anticancer drugs: A guide for nonclinical studies. *Clin. Cancer Res.* **23**, 3489–3498 (2017).
65. FDA, Highlights of Prescribing Information: Carfilzomib; www.accessdata.fda.gov/drugsatfda_docs/label/2012/202714lbl.pdf.
66. Center for drug evaluation and research, application number: 208462Orig1s000 clinical pharmacology and biopharmaceutics review(s) (Ixazomib). (https://www.accessdata.fda.gov/drugsatfda_docs/nda/2015/208462Orig1s000ClinPharmR.pdf).
67. J. Grillo, R. M. Lubin, P. D. CP TL Julie Bullock, P. D. Pharmacometrics Reviewer Li Zhang, H. Li, Office of clinical pharmacology review, (https://www.accessdata.fda.gov/drugsatfda_docs/nda/2012/203469orig1s000clinpharmr.pdf).
68. FDA, Highlights of Prescribing Information: Venetoclax; www.accessdata.fda.gov/drugsatfda_docs/label/2018/208573s009lbl.pdf.
69. FDA, Highlights of Prescribing Information: Trametinib; www.accessdata.fda.gov/drugsatfda_docs/label/2014/204114s001lbl.pdf.
70. A. Naing, C. Aghajanian, E. Raymond, D. Olmos, G. Schwartz, E. Oelmann, L. Grinsted, W. Burke, R. Taylor, S. Kaye, R. Kurzrock, U. Banerji, Safety, tolerability, pharmacokinetics and pharmacodynamics of AZD8055 in advanced solid tumours and lymphoma. *Br. J. Cancer* **107**, 1093–1099 (2012).
71. L. M. Smyth, K. R. Monson, K. Jhaveri, A. Drilon, B. T. Li, W. Abida, G. Iyer, J. F. Gerecitano, M. Gounder, J. J. Harding, M. H. Voss, V. Makker, A. L. Ho, P. Razavi, A. Iasonos, P. Bialer, M. E. Lacouture, J. B. Teitcher, J. P. Erinjeri, N. Katabi, M. G. Fury, D. M. Hyman, A phase 1b dose expansion study of the pan-Class I PI3K inhibitor buparlisib (BKM120) plus carboplatin and paclitaxel in PTEN deficient tumors and with dose intensified carboplatin and paclitaxel. *Invest. New Drugs* **35**, 742 (2017).
72. A. Dobin, C. A. Davis, F. Schlesinger, J. Drenkow, C. Zaleski, S. Jha, P. Batut, M. Chaisson, T. R. Gingeras, STAR: Ultrafast universal RNA-seq aligner. *Bioinformatics* **29**, 15–21 (2013).
73. T. Stuart, A. Butler, P. Hoffman, C. Hafemeister, E. Papalexi, W. M. Mauck, Y. Hao, M. Stoeckius, P. Smibert, R. Satija, Comprehensive integration of single-cell data. *Cell* **177**, 1888–1902.e21 (2019).
74. Z. Gu, R. Eils, M. Schlesner, Complex heatmaps reveal patterns and correlations in multidimensional genomic data. *Bioinformatics* **32**, 2847–2849 (2016).
75. A. Bate, M. Lindquist, I. R. Edwards, S. Olsson, R. Orre, A. Lansner, R. M. De Freitas, A Bayesian neural network method for adverse drug reaction signal generation. *Eur. J. Clin. Pharmacol.* **54**, 315–321 (1998).
76. G. N. Norén, J. Hopstadius, A. Bate, Shrinkage observed-to-expected ratios for robust and transparent large-scale pattern discovery. *Stat. Methods Med. Res.* **22**, 57–69 (2013).
77. J.-E. Salem, T. Yang, J. J. Moslehi, X. Waintraub, E. Gandjbakhch, A. Bachelot, F. Hidden-Lucet, J.-S. Hulot, B. C. Knollmann, B. Lebrun-Vignes, C. Funck-Brentano, A. M. Glazer, D. M. Roden, Androgenic effects on ventricular repolarization: A translational study from the international pharmacovigilance database to iPSC-cardiomyocytes. *Circulation* **140**, 1070–1080 (2019).

78. J.-E. Salem, A. Manouchehri, M. Bretagne, B. Lebrun-Vignes, J. D. Groarke, D. B. Johnson, T. Yang, N. M. Reddy, C. Funck-Brentano, J. R. Brown, D. M. Roden, J. J. Moslehi, Cardiovascular toxicities associated with ibrutinib. *J. Am. Coll. Cardiol.* **74**, 1667–1678 (2019).

**Acknowledgments:** We thank the members of our laboratories for comments and suggestions on this work. **Funding:** This work was supported by funding from the HSPH Dean's Fund for Scientific Advancement (to K.A.S.); HSPH National Institute for Environmental Health Sciences (NIEHS) Center grant P30ES000002 (to K.A.S. and J.K.E.S.); NIH grants R00CA188679 (to K.A.S.), R37CA248565 (to K.A.S.), and R01DK125263 (to K.A.S.); Alex's Lemonade Stand Foundation for Childhood Cancers (to K.A.S.); Andrew McDonough B+ Foundation (to K.A.S.); and Blavatnik Institute at Harvard (to K.A.S.). **Author contributions:** Conceptualization: J.K.E.S. and K.A.S. Methodology: J.K.E.S., M.H.C.F., M.F., J.-E.S., and K.A.S. Formal analysis: J.K.E.S., J.-E.S., and K.A.S. Investigation: J.K.E.S., M.H.C.F., C.S.F., X.Q., J.C., S.J.Y., R.S., M.F., and J.-E.S. Resources: L.L.R., J.-E.S., J.J.M., and K.A.S. Data curation: J.K.E.S., J.-E.S., J.J.M., and K.A.S. Visualization: J.K.E.S. and K.A.S. Funding acquisition: J.K.E.S. and K.A.S. Project administration: K.A.S. Supervision: K.A.S. Writing—original draft: J.K.E.S. and K.A.S. Writing—review and editing: All authors. **Competing interests:** The authors declare that they have no competing interests. **Data and materials availability:** All data needed to evaluate the conclusions in the paper are present in the paper and/or the Supplementary Materials. Gene expression data from this study were deposited in NCBI's GEO (GEO accession GSE188240). VigiBase contains reports of suspected adverse reactions to medicinal products from National Centers in countries participating in the World Health Organization (WHO) pharmacovigilance network, the WHO Programme for International Drug Monitoring (PIDM). The supplied data from VigiBase come from various sources, both regulated and voluntary. Some National Centers accept reports only from medical practitioners; other National Centers accept reports from a broader range of reporters, including patients. Some National Centers include reports from pharmaceutical companies in the information submitted to VigiBase; other National Centers do not. The volume of reports for a particular medicinal product may be influenced by the extent of use of the product, publicity, the nature of the reactions, and other factors. No information is provided on the number of patients exposed to the product. The likelihood of a causal relationship is not the same in all reports. The information does not represent the opinion of WHO.

Submitted 10 December 2021
Accepted 22 September 2022
Published 9 November 2022
10.1126/sciadv.abn6579